Acta Geotechnica
https://doi.org/10.1007/s11440-018-0660-7

RESEARCH PAPER

Effectiveness of deep cement mixing walls with top-down construction for deep excavations in soft clay: case study and 3D simulation

Pitthaya Jamsawang[1] · Panich Voottipruex[2] · Pornpot Tanseng[3] · Pornkasem Jongpradist[4] · Dennes T. Bergado[5]

Received: 6 October 2017 / Accepted: 17 April 2018

Abstract
This paper presents the observed and simulated effectiveness of deep cement mixing walls created using top-down (DCM-TD) construction techniques for a deep excavation in soft Bangkok clay. The wall system consisted of four rows of 0.7-m-diameter DCM columns, and the bracing system consisted of two 0.25-m-thick basement slabs and seven temporary struts. The effectiveness of the wall system compared to that of other wall systems was evaluated using the measured results of previous case studies. A 3D numerical analysis was performed to calculate forces in the basement slabs and bending moments in the DCM wall. Finally, series of parametric analyses of both DCM-TD and deep cement mixing walls created using bottom-up (DCM-BU) construction techniques were carried out, and their results were compared to highlight the effectiveness of DCM-TD and its applicability to excavations at greater depths. The field and numerical results show that DCM-TD is more effective than DCM-BU in terms of the limitations of lateral wall movement, the bending moment in a DCM wall and the thickness of a DCM wall for various depths because of a larger system stiffness. Therefore, DCM-TD is very effective and suitable for use in potential future deep excavations in urban areas.

Keywords Deep excavation · Deep mixing · Finite element · Simulation · Top-down construction in three dimensions · Wall

1 Introduction

Numerous deep excavation projects involving the development of basements for high-rise buildings have been carried out in Bangkok, Thailand, over the past 10 years because of the rapid increase in the economy and size of the city. Deep excavations in soft clays are frequently performed near other buildings and infrastructure [42]. To protect adjacent properties, proper retention systems and construction techniques are required. In the bottom-up (BU) construction technique, sheet pile walls (SPWs), contiguous pile walls (CPWs), and diaphragm walls (DWs) are commonly used as retention systems. SPWs are among the most commonly used to support deep excavations because of their low operational costs, but serious problems may occur, such as larger displacements due to low structural stiffnesses and/or ground movement due to pile driving and extraction. The use of CPWs and DWs comprising thick cast-in-place reinforced concrete walls in the ground can avert the problems of SPWs, but the costs of

✉ Pitthaya Jamsawang
pitthaya.j@eng.kmutnb.ac.th

[1] Department of Civil Engineering, Soil Engineering Research Center, King Mongkut's University of Technology North Bangkok, Bangkok, Thailand

[2] Department of Teacher Training in Civil Engineering, King Mongkut's University of Technology North Bangkok, Bangkok, Thailand

[3] Department of Civil Engineering, Suranaree University of Technology, Nakhon Ratchasima, Thailand

[4] Department of Civil Engineering, Faculty of Engineering, King Mongkut's University of Technology Thonburi, Bangkok, Thailand

[5] School of Engineering and Technology, Asian Institute of Technology, Khlong Nueng, Thailand

Published online: 25 April 2018

such concrete walls are relatively high [38]. Deep cement mixing (DCM) and stiffened DCM (SDCM) walls, which are alternative retaining structures used in BU construction, have been introduced to support deep excavations in soft clays over the past 20 years in Scandinavia, Japan, Germany, the USA and Asia [16]. In a DCM wall, the columns are formed by mixing in situ soil with cement. A DCM wall will typically have a thick cross section due to its low tensile strength and is typically excavated without struts. SDCM walls, which are constructed by inserting steel H-beams into DCM columns to increase the bending moment capacity, are an improvement over DCM walls [15]. Thus, the thickness of a DCM wall can be reduced [42].

The top-down (TD) construction method is used for deep excavations in urban areas when there are extremely strict environmental protections, insufficient working space and extremely short construction times. One advantage of this method is that a basement excavation and a support from the critical path of the project can be removed after the walls and pile foundations are constructed and the first slab is cast. The slabs act as permanent lateral braces for the wall, which are considerably stiffer than cross-lot braces and should minimize adjacent ground movements typically encountered in BU construction [2]. Long [27] summarized the performances of 300 case histories of deep excavations and found no discernible differences in the magnitudes of ground movements associated with both methods. Moormann [29] presented a database of 530 case histories of deep excavations, most of which were through soft soils. The influence of the type of excavation method on performance suggested that the TD systems tended to result in smaller movements than the BU methods. Wang et al. [42] presented a database of 300 case histories of deep excavations through soft soils in Shanghai. The walls that were constructed using the TD method included DWs, CPWs, and SDCM walls, whereas SPWs and DCM walls were constructed using the BU method. They concluded that the TD methods generally resulted in smaller lateral wall displacements. Much research has been conducted using three-dimensional (3D) finite element analysis to investigate the performances of excavations involving DWs, CPWs and SDCM walls with the TD and BU methods in terms of lateral wall movement and settlement behind the walls [10–12, 14, 17, 23, 24, 32, 45]. However, few studies on the performance of DCM walls for deep excavations with TD (DCM-TD) construction in soft clays have been conducted using field observations and numerical investigations.

This paper focuses on evaluations of the effectiveness of a DCM-TD when applied to a deep excavation in soft clay based on a field case study in Bangkok, Thailand. In the field case study, lateral movement profiles around the perimeters of the excavation area and strut forces were observed during the final stage of excavation. The effectiveness of DCM-TD in comparison with other support systems is assessed quantitatively based on field observation data. 3D finite element analysis is used for further investigation. The numerical analysis simulates the lateral wall movement and axial forces in the struts and calculates the force in the concrete slab and the bending moments in the DCM wall induced during excavation. Finally, an investigation of the effect of DCM wall thickness on the lateral movement and bending moment of a DCM wall for excavations at depths greater than that of the case study is numerically carried out to assess the effectiveness and applicability of DCM-TD compared to deep cement mixing walls using the bottom-up (DCM-BU) method.

2 Subsoil conditions

The project construction site was located along Sukhumvit road in central Bangkok, Thailand. The soil profile at this site was a 2-m-thick weathered crust underlain by an 11-m-thick soft clay, a 3-m-thick medium stiff clay, a 14-m-thick stiff clay, and a thick dense sand layer, as shown in Fig. 1a. Detailed laboratory tests were conducted prior to construction to evaluate the geotechnical engineering properties of the foundation soils. The basic physical properties of the tested soils, including natural water content (w_n), liquid limits (LL), plastic limits (PL), wet unit weight (γ), soil specific gravity (G_s) and initial void ratio (e_o), were also characterized. Undrained shear strengths (s_u) obtained from unconfined compression tests were used to characterize the clay types based on strength. These basic properties of the foundation soils are tabulated in Table 1. Conventional oedometer tests and conventional triaxial tests based on consolidated undrained tests were performed on foundation soil specimens taken from the project site at depths of − 1.5, − 7, − 14 and − 18 m for the weathered crust, soft clay, medium stiff clay and stiff clay, respectively, to determine the soil parameters for the numerical simulations. The geotechnical engineering properties of the soils are summarized in the soil profile presented in Fig. 1b–f. The results of the triaxial tests indicate that the effective friction (ϕ') varied from 23° to 28°, whereas the effective cohesion (c') varied from 2 to 30 kPa. These shear strength parameters are consistent with the values for the numerical modeling of Bangkok clays presented in Jamwawang et al. [17]. The ratio of the swelling index (c_s) to the compression index (c_c) obtained from the oedometer tests ranged from 0.13 to 0.25 for stiff and soft clays, which falls within the range of c_s/c_c for the Bangkok subsoils reported by Bergado et al. [3]. The OCR profiles determined based on the oedometer tests show that the weathered crust, medium

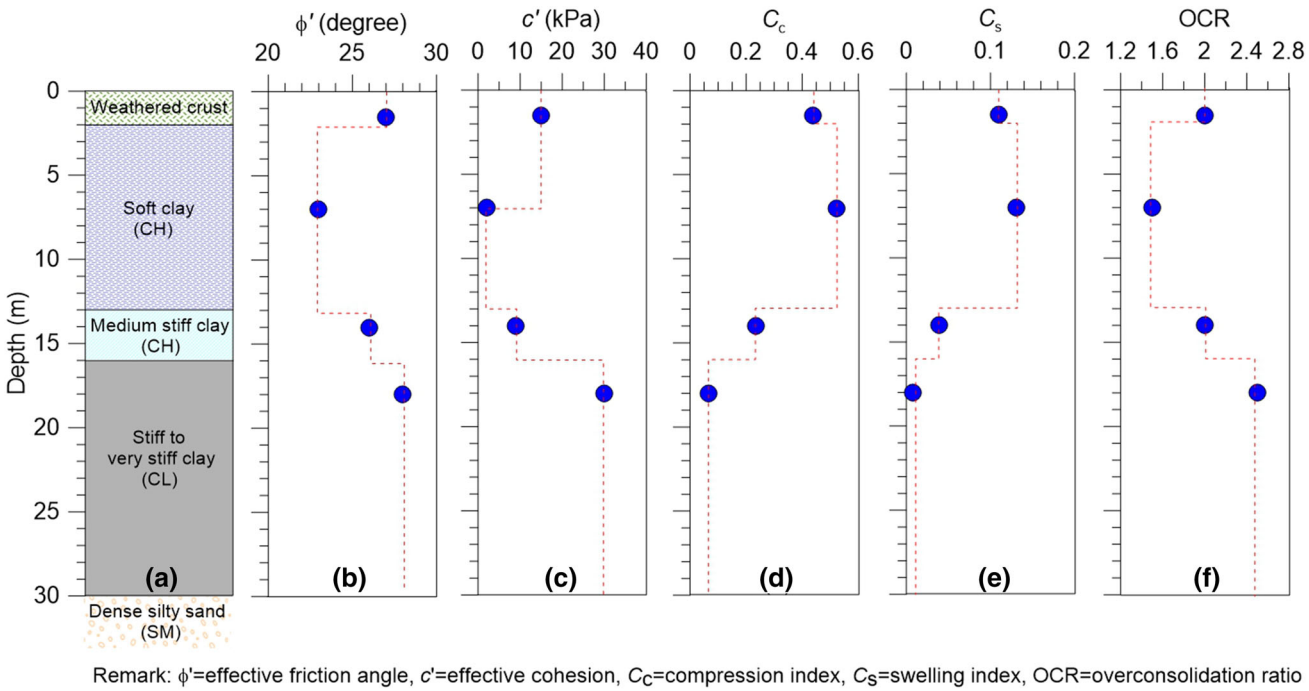

Fig. 1 Soil profiles and soil properties

Table 1 Basic properties of the foundation soils

Depth (m)	Foundation soils	w_n (%)	LL (%)	PL (%)	γ (kN/m^3)	G_s	e_o	s_u (kPa)
0–2	Weather crust	40	58	27	15.5	2.65	1.1	25
2–13	Soft clay	55–72	63–76	27–32	14.5–16.2	2.62–2.68	1.4–1.9	15–20
13–16	Medium stiff clay	48–55	60–73	29–32	16.6–18.1	2.66–2.68	1.2–1.4	25–50
16–30	Stiff to very stiff clay	22–36	40–70	27–32	18.1–18.8	2.65–2.70	0.6–1.0	75–200

stiff clay and stiff clay were heavily overconsolidated and that the soft clay was slightly overconsolidated.

3 Project details

The project involved an 18-story condominium with two underground parking garages, with a maximum excavation depth of 7.90 m. The excavation area involved only the soft clay layer. With insufficient space to construct a thick gravity DCM wall, a DCM wall with temporary bracing systems was designed to reduce the wall thickness. The TD construction technique was used to minimize the construction time, with a permanent basement slab serving as the lateral support. Figure 2a shows the layout of the DCM wall and pile foundation and the locations of the temporary struts. Figure 2b presents the cross section of the DCM wall. The maximum and minimum excavation depths were 7.9 and 6.3 m on the western and eastern sides, respectively, of the excavation area, which were close to a public road and a 2-story building. In addition, an 8-story building and a public road were adjacent to the southern and northern sides of the excavation area, respectively. Within this limited space surrounded by adjacent structures, a performance-based design was adopted. A performance-based design is one that is mainly based on the serviceability of an excavation support system with consideration of the fact that the induced deformation and stress must satisfy the design requirement of a project. Based on past experience related to the design of deep excavation works in the urban Bangkok area, the maximum allowable lateral movement is 65 mm. Within the range bounded by this value, no damage to the ground near the excavation area induced by the slab was found. Another requirement for temporary structural members is a minimum safety factor of 1.50.

The project involved two basements: B1 and B2. The levels of the two basement slabs were different; the B1-A

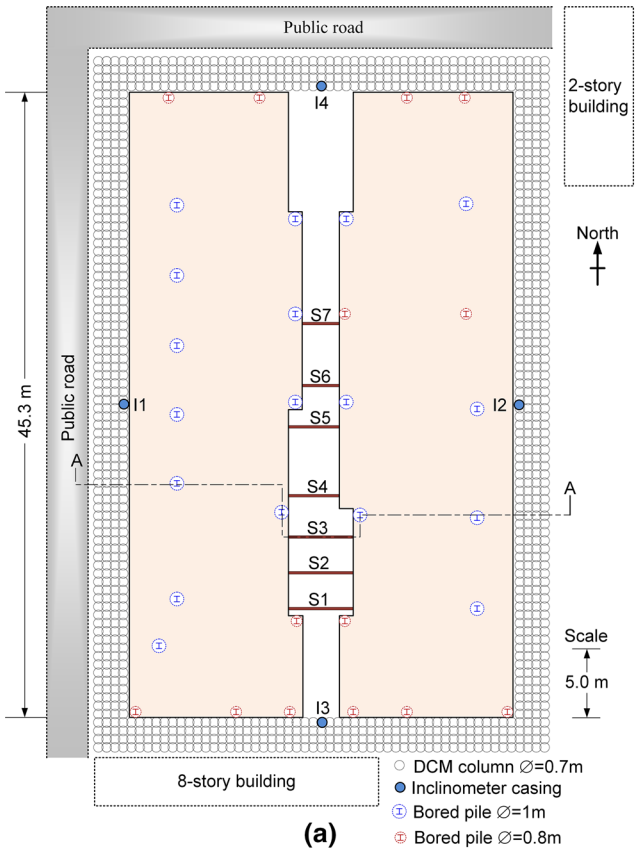

(a)

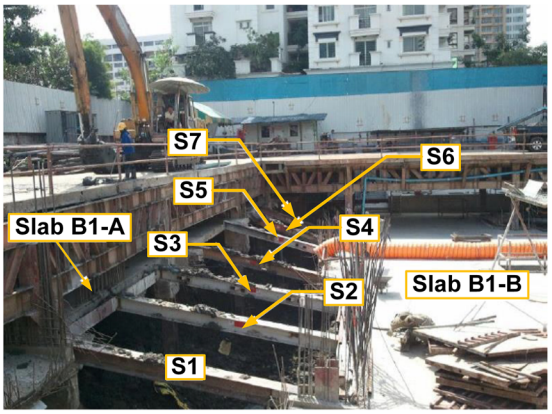

(c)

Strut No.	Strut length, L (m)	Angle, θ (degree)
S1	5.0	19
S2	5.0	19
S3	5.0	19
S4	4.0	24
S5	4.0	24
S6	3.2	30
S7	3.2	30

(d)

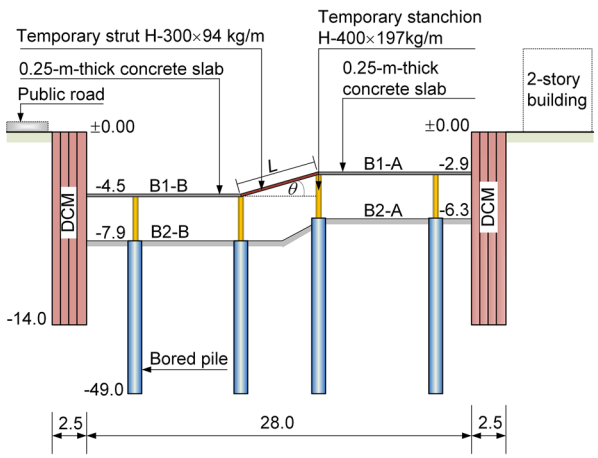

(b)

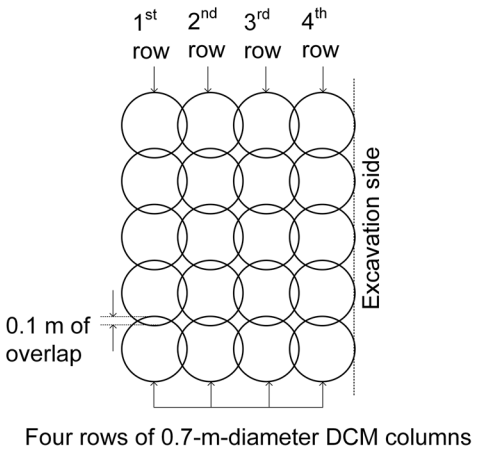

(e)

Fig. 2 **a** Plane view of the excavation area, **b** cross-sectional view A–A of the excavation, **c** DCM wall during TD construction, **d** details of struts and **e** enlargement of the DCM wall

slab was at a level of − 2.9 m, while the B1-B slab was at a level of − 4.5 m. The excavation for B2 was unequal; for the B2-A side, the excavation level was at − 6.3 m, whereas the excavation level for the B2-B side was − 7.9 m. Because the construction employed the TD method, the B1-A and B1-B basement slabs were used as lateral supports between the southern and northern sides of the DCM wall, and they were installed before the construction of the mat foundation. The basement slabs were posttensioned concrete slabs with a thickness and an ultimate compressive strength of 0.25 m and 35 MPa, respectively. In addition, seven temporary struts were connected between the two slabs B1-A and B1-B to act as bracings for transferring the lateral forces induced on the

western and eastern sides of the wall. Notably, the struts used in this project had different lengths and were installed with different inclinations to the horizontal level, as shown in Fig. 2c and d. Finally, temporary stanchions, which were embedded into the bored piles prior to the excavation work, were required to support the basement slabs. The DCM wall used at this site comprised four rows of 0.7-m-diameter DCM columns with 0.1 m of overlap, an enlarged view of which is shown in Fig. 2e. The entire thickness of the DCM walls was 2.5 m, and the tip was − 14.0 m from the ground surface. The DCM wall tip was embedded 1 m into the medium stiff clay layer. The DCM walls were installed using a low-pressure mechanical mixing method. The cement content was 250 kg/m^3 of wet soil, and the water/cement ratio was 1.1. Figure 2e also shows the construction sequences of the DCM walls. The first row, which is farthest from the excavation side, was first constructed to prevent lateral movement induced by the installation of subsequent rows of the DCM columns. Then, the second, third and fourth rows were installed.

After the DCM wall construction was completed, core samples were extracted from the DCM columns at various depths in three locations, C-1, C-2 and C-3, for the laboratory tests. Figure 3 presents the test results of the core samples. The bulk unit weights ranged from 15 to 16.5 kN/m^3, and the moisture content varied from 35 to 70%. The unconfined compressive tests were performed on samples 50 mm in diameter and 100 mm in height. The unconfined compressive strengths of the DCM columns, $q_{u(DCM)}$, ranged from 1.4 to 2.1 MPa, with an average value of 2.0 MPa, whereas the moduli of elasticity (E_{DCM}) ranged from 120 to 290 MPa, with an average value of 200 MPa, indicating an empirical relationship $E_{DCM} = 100\ q_{u(DCM)}$, corresponding to the test results of Huang and Han [13], Jongpradist et al. [20] and Jamsawang et al. [15–19].

The excavation stages versus construction periods are listed in Table 2. A waiting period of 3 days was required for the strength of the concrete slabs to reach 60% of the ultimate design strength (35 MPa) before the next stage of excavation was performed. The strength and stiffness of the concrete slabs at 60% of the ultimate design strength are sufficient for them to function as wall bracings [2]. After the floor zone B2-B was completely installed, a lean concrete was immediately poured to create permanent lateral bracings. In addition, permanent reinforced concrete walls and columns covering the stanchion were constructed. All stages of the excavation work are illustrated in Fig. 4. With a good design construction sequence for a moderate excavation depth of approximately 7.9 m with two basement levels, the excavation could be successfully accomplished in 88 days, with an average construction period of 7 days for each excavation stage. Arboleda-Monsalve and Finno [2] recorded the lateral movement of walls during a 15-m-depth deep excavation via TD construction in clayey soils. The entire excavation construction period was 480 days, with an average construction period of 45 days for each excavation stage. Field measurement data showed that creep effects represented approximately 30% of the maximum measured lateral wall movement, whereas the remaining 70% arose from stress relief. Due to the short average construction period, the creep effect, which may play an important role in long-term deep excavations, was thus minimal in this project and can be disregarded. Figure 23 illustrates that the creep effect provided only 7% of the maximum observed lateral wall movement, with the remaining 93% caused by stress relief.

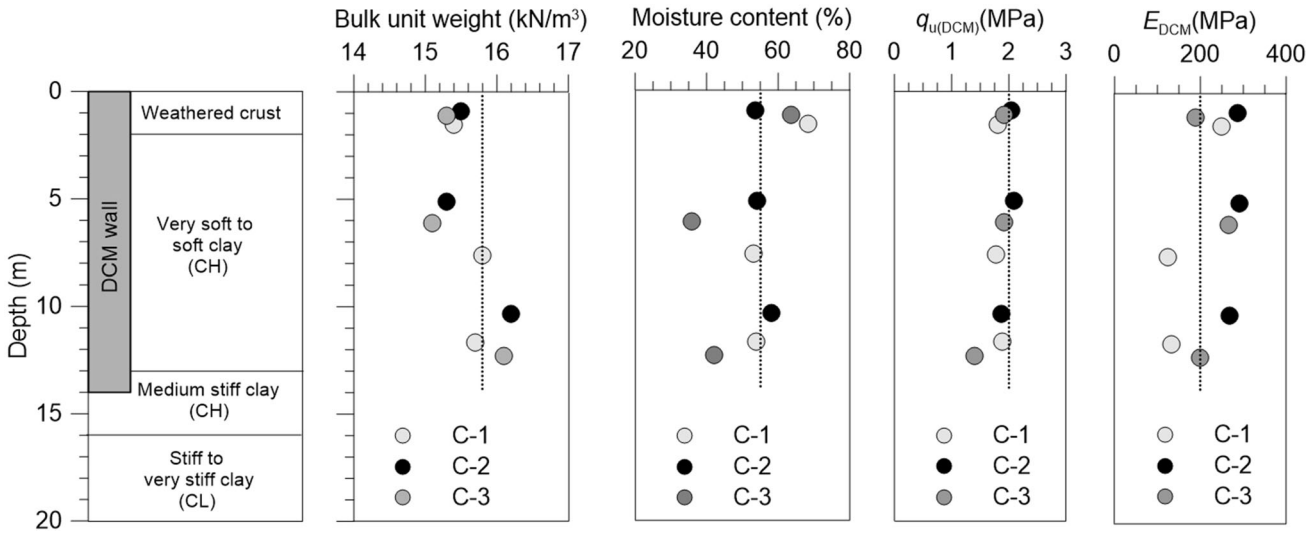

Fig. 3 Properties of the cored DCM columns

Table 2 Excavation stages versus construction period

Stage	Detail	Duration (days)
1	Construct 0.7- and 0.8-m-diameter bored piles to support the structural load	–
2	Install a temporary column (stanchion) using H-400 × 197 kg/m steel embedded into the bored piles to transfer the weight from the basement floor during construction to the bored piles	–
3	Install DCM column walls by deep wet mixing around the excavated area to be used as a temporary retaining structure for the construction of the basement	–
4	Excavate to − 3.20 m for floor zone B1-A	5
5	Install concrete slab zone B1-A	2
6	Wait for strength development of concrete slab zone B1-A	3
7	Excavate to − 4.80 m for floor zone B1-B	15
8	Install concrete slab zone B1-B	2
9	Wait for strength development of concrete zone B1-B	3
10	Install temporary struts between slab zones B1-A and B1-B using H 300 × 94 kg/m steel to transfer the lateral load due to the excavation	2
11	Excavate to − 6.30 m for space between floor zones B1-B and B1-A	5
12	Excavate to − 6.30 m for floor zone B2-A	28
13	Excavate to − 7.90 m for floor zone B2-B	23
	Total	88

Four inclinometer casings were installed up to the stiff clay layer at a depth of 19.0 m, which is approximately 2.5 times the excavation depth (H_e) and is sufficient to obtain a zero reading at this depth based on the practical work related to deep excavation projects in soft Bangkok clay reported by Likitlersuang et al. [23]. Inclinometer casings were installed in the middle of the walls on four sides of the excavation boundary to monitor the lateral wall movement, as shown in Fig. 2a. To measure the forces in the temporary struts installed between B1-A and B1-B and to avoid the bending stress component, electrical strain gauges were attached to the neutral axes of the struts. A dummy strain gauge was used to eliminate any effect of temperature. No prestressed loading of the struts was performed for this project.

4 Numerical analysis of the field case study

4.1 Finite element mesh and boundary condition

A finite element simulation using the PLAXIS 3D version 2013 software was conducted to describe the performance of the DCM wall. The 3D finite element model comprised the DCM columns, bored piles and foundation soils. The soil volume was modeled using ten-node tetrahedral volume elements. The circular columns (bored piles) were modeled as prismatic columns with square cross-sectional areas and diameters of 0.8 and 1.0 m. The stanchions and struts (Fig. 2a and b) were modeled using beam elements, whereas the basement slabs (Fig. 2a and b) were modeled using plate elements. Figure 5a and b illustrates the 430,000-element 3D finite element mesh used in the analysis, which corresponds to the DCM wall configuration in Fig. 2a and b. At the bottom of the finite element mesh, the displacements were set to zero in the *x*-, *y*- and *z*-directions. The vertical model boundaries were fixed in the *x*- and *y*-directions and free in the *z*-direction. To avoid boundary effects, the length and width of the model were chosen to be 160 and 140 m, respectively, and its depth was 30 m.

4.2 Constitutive model and model parameters

The hardening soil model is an advanced model for simulating the behavior of different types of soft and stiff soils [16–19, 33, 37, 39, 43, 44, 46] and was used to simulate the behavior of the weathered crust, soft clay, medium stiff clay, stiff clay and DCM column in this study. Schanz et al. [36] explained in detail that the most significant features of the present hardening soil model are the use of a hyperbolic stress–strain curve and the control of the stress-level dependency because the stiffness of real soils depends on the stress level. The theory of plasticity [4], soil dilatancy and a yield cap are also applied in the model. Thus, the yield surface is able to expand due to plastic strain. Hardening processes can be divided into two main types: compression and shear. The former is used for modeling

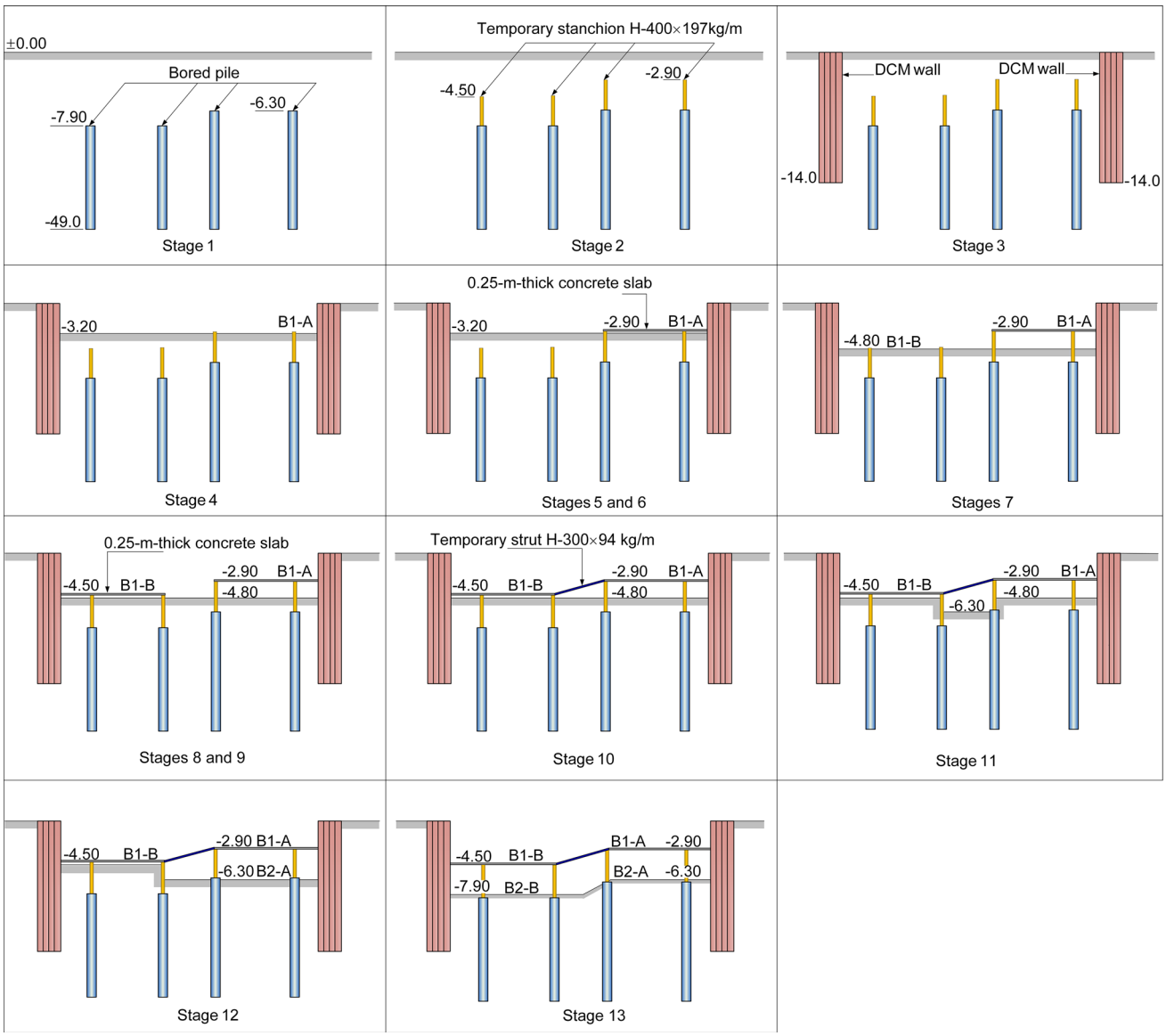

Fig. 4 Stages of the excavation construction

the irreversible plastic strains caused by primary compression in oedometer and isotropic loadings, whereas the latter is employed for modeling irreversible strains due to primary deviatoric loading. A soil that is subjected to primary deviatoric loading exhibits a decrease in stiffness, and irreversible plastic strains concurrently develop.

The stress–strain relationship due to the primary loading is assumed to be a hyperbolic curve in the hardening soil model. The hyperbolic function for the drained triaxial test can be formulated as

$$-\varepsilon_1 = \frac{1}{E_i}\frac{q}{1-q/q_a} \quad \text{for } q < q_f \tag{1}$$

where q_a is the asymptotic value of the shear strength, and E_i the initial stiffness. E_i is related to E_{50} by

$$E_i = \frac{2E_{50}}{2-R_f} \tag{2}$$

This relationship is plotted in Fig. 6. The parameter E_{50} is the confining stress-dependent stiffness modulus for primary loading, which is 50% of the secant stiffness modulus and is given by the equation

$$E_{50} = E_{50}^{\text{ref}}\left(\frac{c'\cos\phi' - \sigma_3'\sin\phi'}{c'\cos\phi' + p^{\text{ref}}\sin\phi'}\right)^m \tag{3}$$

where E_{50}^{ref} is a reference stiffness modulus corresponding to the reference confining pressure, p^{ref}, of 100 kPa. The actual stiffness depends on the minor principal stress, σ_3', which is the confining pressure in a triaxial test. The amount of stress dependency is given by the power

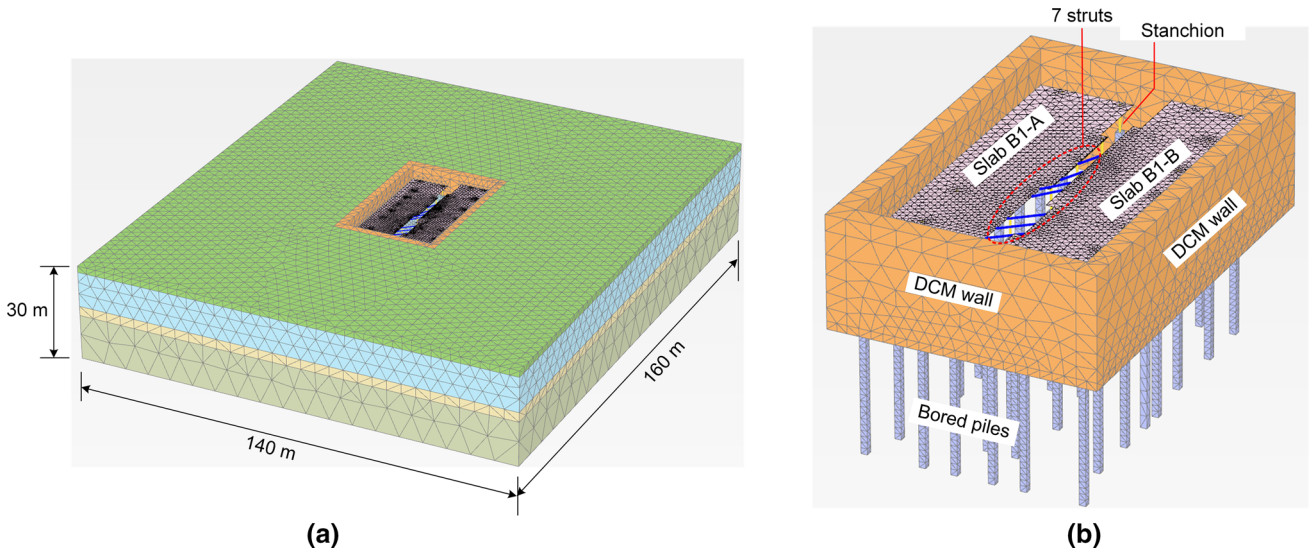

Fig. 5 **a** 3D finite element mesh of the wall and **b** enlargement of the modeling excavation area

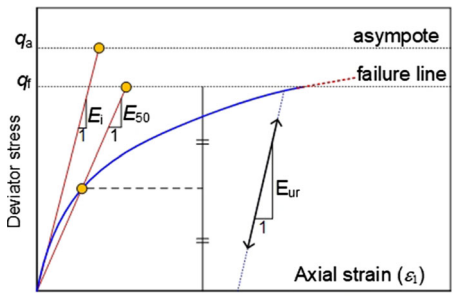

Fig. 6 Hyperbolic stress–strain relation in primary loading for a standard drained triaxial test (Schanz et al. [36])

m. Surarak et al. [39] reported a range of m values from 0.5 to 1 for different soil types, with values of 0.9–1 for clayey soils. The ultimate deviatoric stress, q_f, and the quantity q_a in Eq. (1) are defined as

$$q_f = (c' \cot \phi' - \sigma_3') \frac{2 \sin \phi'}{1 - \sin \phi'} \tag{4}$$

$$q_a = \frac{q_f}{R_f} \tag{5}$$

The above relationship for q_f is derived from the Mohr–Coulomb failure criterion, which involves the strength parameters c′ and ϕ'. The ratio between q_f and q_a is given by the failure ratio R_f, which should clearly be smaller than 1. An R_f of 0.9 is chosen as a suitable value for various soil types [16–19, 33, 37, 39, 43, 44, 46]. For the unloading and reloading stress paths, another stress-dependent stiffness modulus is used:

$$E_{ur} = E_{ur}^{ref} \left(\frac{c' \cos \phi' - \sigma_3' \sin \phi'}{c' \cos \phi' + p^{ref} \sin \phi'} \right)^m \tag{6}$$

where E_{ur}^{ref} is the reference Young's modulus for unloading and reloading, corresponding to the reference pressure p^{ref} of 100 kPa. The shear hardening yield function, f, in the hardening soil model is given as

$$f = \bar{f} - \gamma^p \tag{7}$$

where $\bar{f}$ is a function of the stress and γ^p is a function of the plastic strain:

$$\bar{f} = \frac{2}{E_i} \frac{q}{1 - q/q_a} - \frac{2q}{E_{ur}} \tag{8}$$

$$\gamma^p = -\left(2\varepsilon_1^p - \varepsilon_v^p\right) \approx -2\varepsilon_1^p \tag{9}$$

$$\varepsilon_1^p \approx \frac{1}{2}\bar{f} = \frac{1}{E_i} \frac{q}{1 - q/q_a} - \frac{q}{E_{ur}} \tag{10}$$

where ε_1^p and ε_v^p are the plastic vertical strain and the plastic volumetric strain, respectively.

In addition to plastic strains, the model also accounts for elastic strains. Plastic strains develop in primary loading alone, but elastic strains develop both in primary loading and in unloading/reloading. For drained triaxial test stress paths with $\sigma_2' = \sigma_3'$ = constant, the elastic Young's modulus E_{ur} remains constant, and the elastic strains are given by

$$-\varepsilon_1^e = \frac{q}{E_{ur}} \tag{11}$$

$$-\varepsilon_2^e = -\varepsilon_3^e = -\nu_{ur} \frac{q}{E_{ur}} \tag{12}$$

where ν_{ur} is the unloading/reloading Poisson's ratio and ε_2^e and ε_3^e are the elastic radial strains. A value of ν_{ur} of 0.2 is typically used in this model [21, 36, 46]. For the deviatoric loading stage of the triaxial test, the axial strain is the sum

Table 3 Parameters used in hardening soil model

	Weathered crust	Soft clay	Medium stiff clay	Stiff clay	DCM column
Unit weight, γ (kN/m^3)	16	15	17	19	16
Secant stiffness, E_{50}^{ref} (kPa)	10,000	1200	10,000	20,000	200,000
Tangential stiffness, $E_{\text{oed}}^{\text{ref}}$ (kPa)	12,000	960	12,000	25,000	150,000
Unloading and reloading stiffness, $E_{\text{ur}}^{\text{ref}}$ (kPa)	35,000	4000	45,000	95,000	600,000
Power of the stress-level dependency of the stiffness, m	1.0	1.0	0.9	0.9	0.9
Poisson's ratio for unloading–reloading, ν_{ur}	0.2	0.2	0.2	0.2	0.2
Effective cohesion, c' (kPa)	15	2	9	30	510
Effective friction angle, ϕ' (degrees)	27	23	26	28	36
Angle of dilatancy, ψ (degrees)	0	0	0	0	0
Over-consolidation ratio, OCR	2.0	1.5	2.0	2.4	–
Material behavior	Undrained	Undrained	Undrained	Undrained	Undrained

of an elastic component given by Eq. (11) and a plastic component obtained from Eq. (10). Hence, it follows that

$$-\varepsilon_1 = \varepsilon_1^{\text{e}} - \varepsilon_1^{\text{p}} \approx \frac{1}{E_{\text{i}}} \frac{q}{1 - q/q_{\text{a}}} \tag{13}$$

Another input parameter, the reference oedometer modulus ($E_{\text{oed}}^{\text{ref}}$), is used to control the magnitude of the plastic strains that originate from the yield cap. In a similar manner to the triaxial moduli, the oedometer modulus (E_{oed}) obeys the stress dependency law

$$E_{\text{oed}} = E_{\text{oed}}^{\text{ref}} \left(\frac{c' \cos \phi' - \frac{\sigma_3'}{K_{\text{o}}^{\text{nc}}} \sin \phi'}{c' \cos \phi' + p^{\text{ref}} \sin \phi'} \right)^m \tag{14}$$

where E_{oed} is a tangent stiffness modulus and K_{o}^{nc} is K_{o} for normal consolidation, which is $1 - \sin \phi'$. The tensile strength of the DCM columns, which were considered using the tension cutoff in the model, was 15% of $q_{\text{u(DCM)}}$ [19]. The linear elastic model was employed to model the behaviors of the concrete slabs, stanchions, struts and bored piles [17]. The parameters of the linear elastic model are listed in Table 3.

4.3 Soil parameter calibration for the foundation soils and DCM columns

The laboratory test results and hardening soil model were calibrated by modeling the triaxial and oedometer tests using a 2D finite element method using axisymmetric geometries of 50 × 25 mm and 10 × 30 mm, as shown in Fig. 7a and b, respectively, to obtain reasonable soil parameters for simulating the field behaviors of the foundation soils. The results of the triaxial tests are presented in the form of the deviator stress versus axial strain, whereas those of the oedometer tests are shown as plots of the

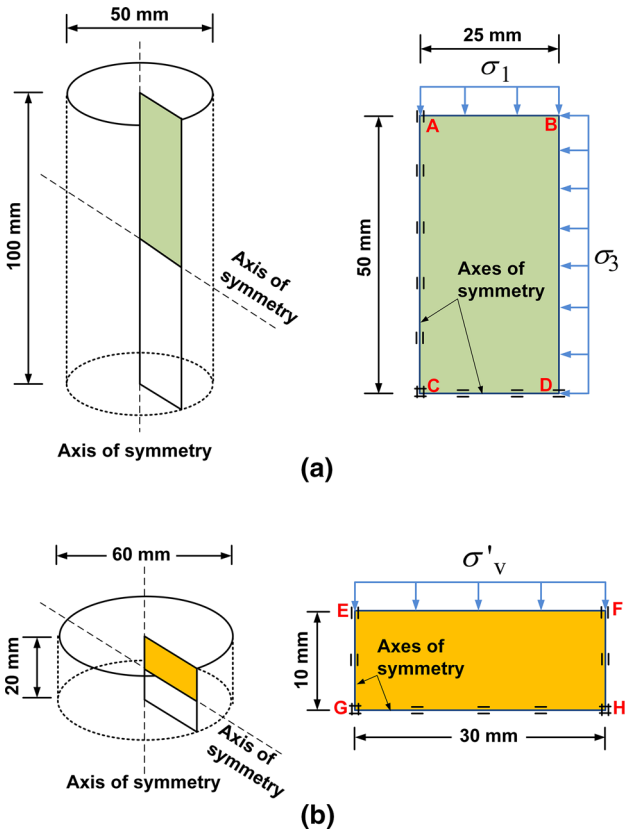

Fig. 7 Simplified geometries of: **a** triaxial test and **b** oedometer test in 2D finite element models

logarithm of the vertical effective stress versus the vertical strain curves, as shown in Fig. 8a–e. These tests included loading and unloading, from which the loading stiffness, the unloading stiffness and the power of the stress-level dependency of the stiffness could be determined [17].

The simplified geometries in the triaxial and oedometer models represent one-quarter of the soil specimens. The

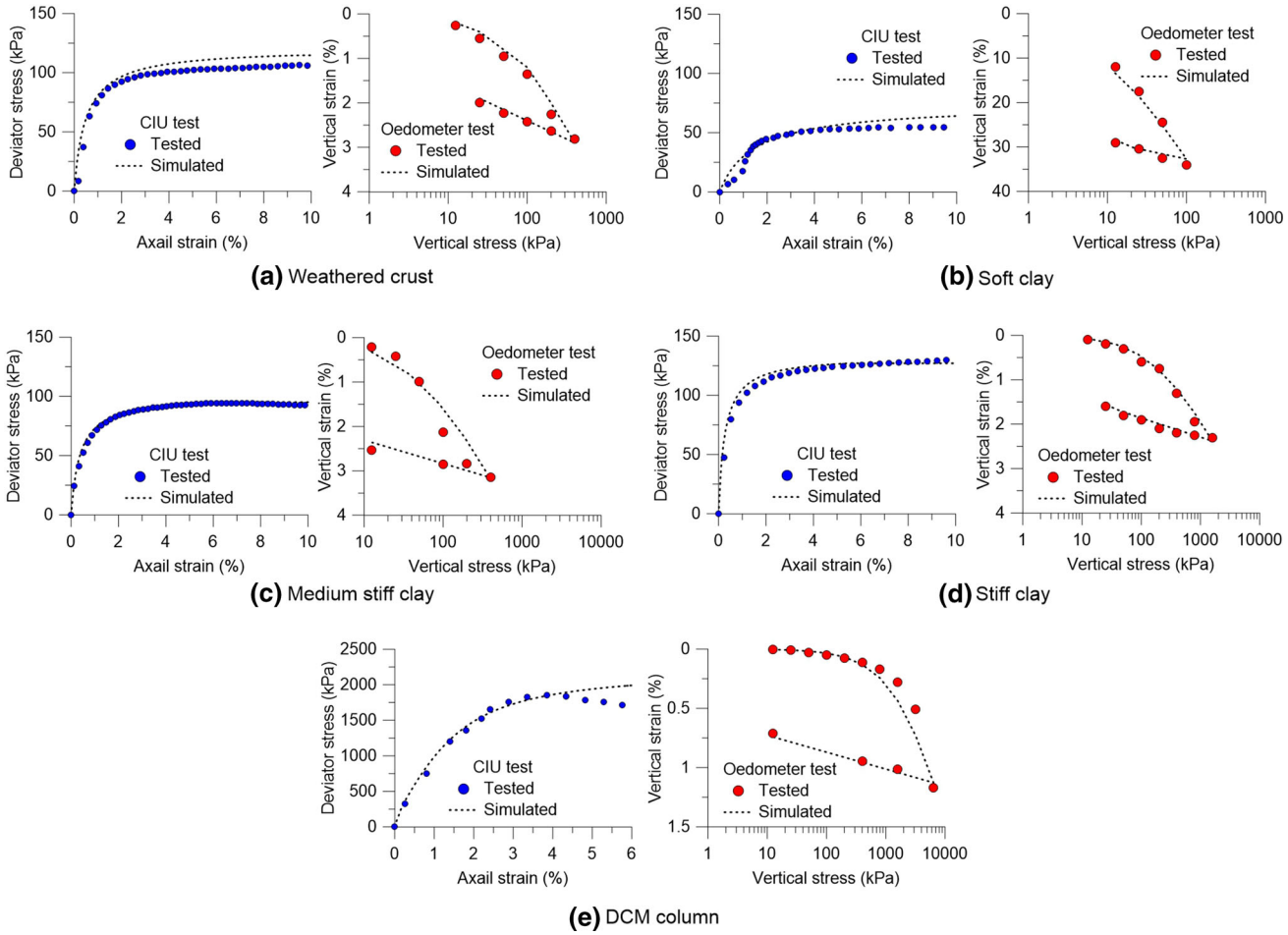

Fig. 8 Soil parameter calibrations

deformations along the boundaries for the triaxial model (lines AC and CD) and for the oedometer model (lines EG, GH and FH) were kept free to allow smooth movement along the axes of symmetry, whereas the deformations perpendicular to the boundaries were fixed. The boundaries AB, BD and EF were free to move. The applied vertical and confining stresses were simulated as distributed load systems σ_1 and σ_3 for the triaxial model, while the applied normal effective stress was simulated as a distributed load system σ'_v for the oedometer model. A 15-node triangular element was selected for this analysis. The clusters, representing a quarter of the soil specimens in both tests, were divided into soil elements during the mesh generation process.

The input shear strength parameters c' and ϕ' for the foundation soils and DCM column were obtained from the triaxial test results. The values of the parameters E_{50}^{ref}, $E_{\text{oed}}^{\text{ref}}$, $E_{\text{ur}}^{\text{ref}}$ and m are independent inputs in the hardening soil model. These parameters were adjusted to obtain suitable values to provide the best-fit results of the stress–strain curves. The results shown in Fig. 8a–e reveal good agreement with the stress–strain curves for the weathered crust, soft clay, medium stiff clay, stiff clay and DCM column, respectively. Therefore, suitable soil parameters of the hardening soil model for the 3D finite element analysis for this study are presented in Table 4. The stiffness parameters used in this study are similar to those derived by Surarak et al. [39] for Bangkok clay.

5 Numerical results and comparisons with measurement data

Because of the limited space of the construction site, only some instruments, i.e., inclinometers and strain gauges, which were used to measure the lateral movements and strut loads, respectively, were installed. A 3D finite element analysis was thus performed with careful consideration of both the material parameters and analysis procedures to generate the responses of the soil and wall, which could not be directly obtained from the field. In this section, the simulated results are compared with the

Table 4 Parameters used in linear elastic model

	Concrete slab	Bored pile	Temporary strut	Stanchion
Unit weight, γ (kN/m^3)	24	24	78	78
Moment of inertia, I (m^4)	1.3×10^{-3} m^4/m	0.012–0.020	2.0×10^{-4}	7.1×10^{-4}
Cross-sectional area, A (m^2)	0.25 m^2/m	0.38–0.50	0.012	0.025
Elastic modulus, E (kPa)	2.8×10^7	2.0×10^7	2.1×10^8	2.1×10^8
Poisson's ratio, ν	0.15	0.15	–	–
Material behavior	Plate element	Non-porous	Beam element	Beam element

measurement data to verify the computed values, which will be discussed later.

5.1 Lateral movement profile

The observed lateral movement profiles of the DCM wall in the middle of each side of the excavation area were obtained from the four inclinometers (shown in Fig. 2a), I1, I2, I3 and I4, at the western, eastern, southern and northern parts of the excavation, respectively. The lateral wall movement profiles of the final stage of the excavation (stage 13) are shown in Fig. 9a–d. In the figures, the computed lateral movement profiles from the 3D finite element analysis are also included for comparison. The trends of the lateral movement profiles were reasonably well captured, and the computed magnitudes were generally in good agreement with the observed data for I1, I2, I3 and I4. The 20% maximum overestimation of the computed δ_{hm} at a depth of 8 m (20 mm) for I4 was 5 mm, whereas the 20% maximum underestimation of the calculated δ_{hm} at a depth of 9 m (15 mm) for I3 was 5 mm.

For the I1 side, the wall movement showed a small curvature, which means that the wall was tilted like a block. The wall was permitted to deflect as a cantilever beam. The maximum lateral wall movement (δ_{hm}) located at the top of the wall (near the ground surface) was 58 mm, and the movement at the tip of the wall (at a depth of 14 m) was 15 mm, which implies that the movement pattern was a combination of slight overturning and sliding. For inclinometer I2, the amount of wall movement was less than that detected by I1 because the excavation depth was smaller. δ_{hm} was 32 mm at the top of the wall, and the movement at the tip of the wall was 10 mm. The lateral movement profiles for the I3 and I4 sides are presented in Fig. 9c and d, respectively. The magnitudes of the lateral movements were considerably smaller than those of the I1 and I2 sides because of the smaller wall length and sufficient lateral support from the concrete slab bracings B1-B and B1-A. Because the final excavation depths (H_e) were the same, there were no significantly different lateral wall deflections on the two sides of I3 and I4. The lateral movement profiles developed into a bulged profile pointed

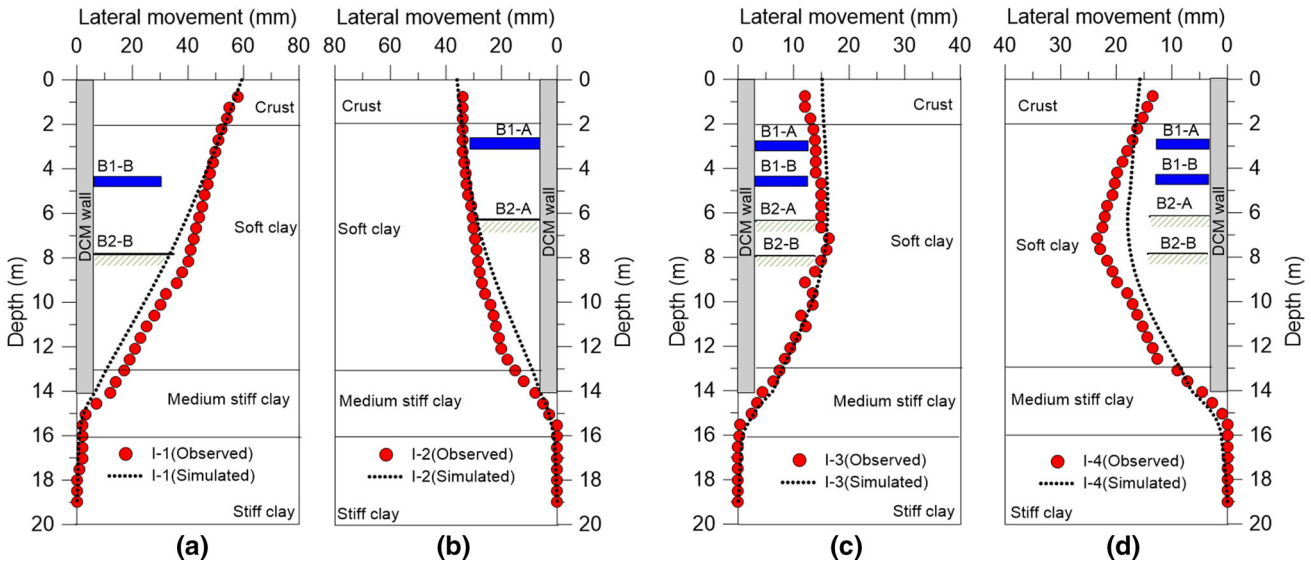

Fig. 9 Comparison of measured and computed lateral wall movements

inward toward the excavation area, indicating that the walls of the two sides were well propped near the surface. Thus, the maximum lateral movement (H_{hm}) occurred at a deeper depth. δ_{hm} was 22 and 26 mm at distances 4.5 and 7 m below the ground surface for the walls associated with I3 and I4, respectively. The tip movements of the retaining wall were only 5 mm for I3 and I4.

H_{hm} was at the ground surface for I1 and I2, whereas it was 0.63 and 1.0 H_e below the ground surface for I3 and I4, respectively. Ou et al. [30] found that the H_{hm} of eight case histories in Taipei soft soil were often observed near the excavation surface. The analysis of Moormann [29] showed that the δ_{hm} for most deep excavations in a soft soil were observed at depths from 0.5 to 1.5 H_e under the ground surface. Wang et al. [42] reported that H_{hm} was observed at depths from 0.5 to 1.0 H_e under the ground surface in 53% of the case histories. For 43% of the case histories, H_{hm} was observed at depths from 1.0 to 1.4 H_e under the ground surface. H_{hm} was observed at the top of the wall for only approximately 4% of the case histories. δ_{hm} for the DCM walls without internal struts occurred at the tops of the walls. Deep-seated wall displacements were observed when internal struts were used to support the DCM walls. The results of Ou et al. [30], Moormann [29] and Wang et al. [42] were broadly confirmed by this study.

The tip movement of the retaining wall was found to occur at I1 and I2. Wang et al. [41] reported that the embedded depth ratio of the wall (D/H_e) may contribute to the toe movement, where D is the embedded length of the wall. D/H_e is an important index that reflects the economy of the retaining wall. It also has some impact on the factor of safety against basal heave. Here, the embedment ratio was $0.77D/H_e$ for the DCM wall and mainly varied between 0.8 and 1.4, being 1.08 on average [41]. Thus, D/H_e was the smallest in this study. A larger D/H_e ratio could help in suppressing the toe movement because more soils under the excavation surface would be strengthened.

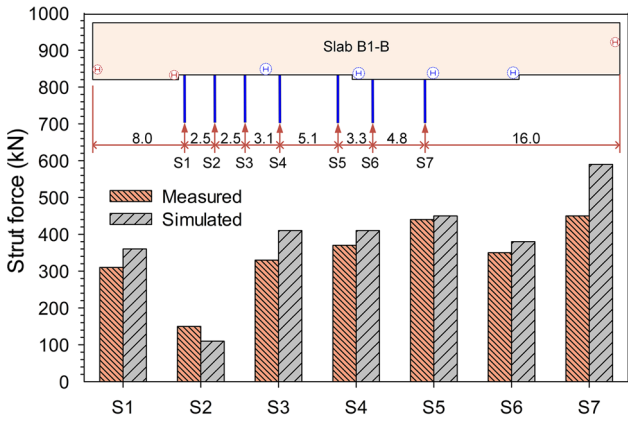

Fig. 10 Comparison of measured and calculated strut forces

5.2 Strut force

Figure 10 shows comparisons of the measured and computed strut forces induced by the 7.9-m-deep excavation for all struts, as shown in Fig. 2a–c. The measured values of the strut forces were 310, 150, 330, 370, 440, 350 and 450 kN, whereas the computed values were 360, 110, 410, 410, 450, 380 and 590 kN for struts S1 to S7, respectively. Strut S7 was farthest from the edge of the slab and experienced a larger axial force than the other struts. The yield strength of the steel used in the struts was 250 MPa, resulting in a yield axial force of 3000 kN. Thus, minimum factors of safety against structural failure of 6.7 and 5.1 were obtained for this project, which were based on measured and simulated values of the strut forces, respectively.

A comparison of the observed and computed data indicated a maximum underestimation of 36% and overestimation of 24% for struts I2 and I7, respectively. However, the average error in the comparison was only 16%. Therefore, the computed magnitudes of the strut forces were generally in good agreement with the observed data. The calculated force in strut S7 was approximately twice the measured and calculated forces in strut S1 because the spacing of S7 was twice the spacing of S1. This shows that the computed strut forces provide reliable results. These comparisons give us confidence in the values computed using the 3D finite element analysis, which will be used later in the discussion.

A strut is generally a compressive structural member (Fig. 11a), but all the struts used in this study were installed with inclinations due to the different levels of the

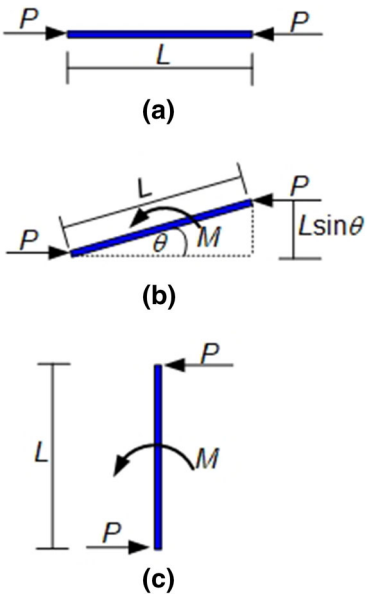

Fig. 11 Orientation of strut with respect to the applied force direction and the induced structural force for: **a** $\theta = 0^o$, **b** $0^o < \theta < 90^o$ and **c** $\theta = 90^o$

two basement slabs. Thus, the excess bending moment induced produces a combination of compressive and tensile stresses in a cross section of the struts instead of pure compression. The excess bending moment can be approximately calculated as the product of the lateral force transferred from the basement slabs, P, and the moment arm, $L\sin\theta$; where L is the strut length and θ is the inclination angle, as shown in Fig. 11b. It can be seen that the strut length and inclination angle have influences on the normal force on the strut section; the greater the value of $L\sin\theta$, the larger the excess bending moment. Considering only the term θ, an increase in θ changes the function of a strut from a compressive to a flexural structural member (Fig. 11c). The numerical results show that the excess couple bending moments induced are 61, 43, 45, 62, 53, 54 and 60 kN-m for struts S1–S7, respectively. However, the excess bending moments were compensated by the high value of the factor of safety against structural failure of 5.1.

5.3 Sensitivity analysis of input soil parameters on the maximum lateral movement

This section presents the results of a sensitivity analysis of the soil parameters used in the model regarding the magnitude of the computed maximum lateral movement obtained from wall I1 to investigate which parameters have the most significant influence on the results. The parameters studied are (1) E_{50}^{ref}, (2) $E_{\text{oed}}^{\text{ref}}$, (3) $E_{\text{ur}}^{\text{ref}}$, (4) m, (5) v_{ur}, (6) c', (7) ϕ' and (8) R_{f}. As mentioned previously, one parameter was varied with respect to the case study in each analysis to determine the influence of that specific parameter. The values of each parameter had error variations from − 50% to 50% of the input values in the case study, as tabulated in Table 3. The computed maximum lateral movement was 60 mm based on the parameters in Table 4. Figure 12 shows the influence of these soil parameters; $E_{\text{ur}}^{\text{ref}}$ has the most influence, providing values of 111 and 44 mm or 185% overestimation and 73% underestimation for percent errors of − 50 and 50, respectively, because of the maximum lateral movement induced by the unloading of the soil weight from the excavation. Thus, $E_{\text{ur}}^{\text{ref}}$ is a main parameter that quickly responds to unloading soil behavior, whereas E_{50}^{ref}, $E_{\text{oed}}^{\text{ref}}$ and c' can be considered insignificant and the rest of the parameters slightly affect the maximum lateral movement. However, all the values of $E_{\text{ur}}^{\text{ref}}$ used in this study are in the range of the test results reported by Surarak et al. [39] for Bangkok clay.

5.4 Discussion of the effectiveness of DCM-TD compared to that of other support systems

The relationship between δ_{hm} and H_{e} in this deep excavation is shown in Fig. 13. The results indicate that the values

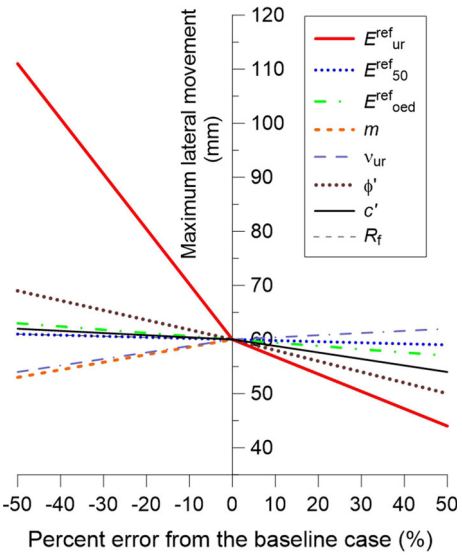

Fig. 12 Sensitivity analysis of input soil parameters on the maximum lateral movement

of δ_{hm} were 0.73, 0.51, 0.23 and 0.33%H_{e} for the walls associated with I1, I2, I3 and I4, respectively. The measured results for all types of supporting systems obtained for the metro excavations in Bangkok and Shanghai soft clays are also shown for comparison because properties of the foundation soils are similar. All types of supporting systems were used, including DWs constructed using the TD method (DW-TD) and using the BU method (DW-BU), DCM walls constructed using the BU method (DCM-BU), and SPWs constructed using the BU method. The results of Wang et al. [42] indicated that the mean values of δ_{hm} for DW-TD, DW-BU, DCM-BU and the SPWs were 0.27, 0.4, 0.91 and 1.5%H_{e}, respectively, whereas the database in the Bangkok area shows that those for DW-TD, DW-BU, DCM-BU and the SPWs were 0.25, 0.31, 1.37 and

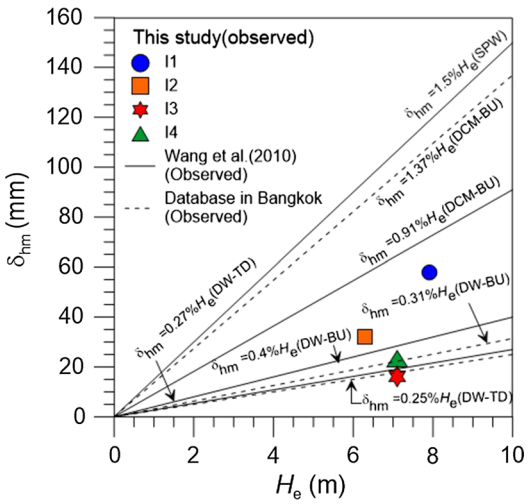

Fig. 13 Observed lateral movement versus excavation depth

1.45%H_e, respectively. Thus, the values of the ratio δ_{hm}/H_e for each type of supporting system used in Bangkok and Shanghai soft clays are similar, except that of DCM-BU, which is different because the quality control of a DCM construction might be different for each country. For the DCM-TD method in this study, the larger values of δ_{hm}/H_e (based on I1 and I2) were between those of DCM-BU and DW-BU, whereas the smaller values of δ_{hm}/H_e (based on I3 and I4) were between those of DW-BU and DW-TD. The type of wall and construction technique used have a significant influence on δ_{hm}, as expected. The values of δ_{hm} for the DCM-BU method were considerably larger than those for any other type of wall, except the SPWs, because the DCM walls were largely excavated in the manner of a cantilever. The δ_{hm} trend was significantly smaller for relatively stiff walls, including the DW-BU and DW-TD. The mean value of δ_{hm} for this study was 0.45%H_e, which is approximately 2 and 3 (or 2.5 (average)) times smaller than the observed values of δ_{hm} for the DCM-BU in Shanghai and Bangkok soft clays, respectively. In addition, the mean value of δ_{hm} for DCM-TD was 0.8 and 0.5 times larger than the average observed values of δ_{hm} for DW-BU and DW-TD, respectively. The observed effectiveness of DCM-TD in comparison with that of DCM-BU was assessed quantitatively in terms of the reduction ratio for the lateral wall movement, which was defined as the ratio of the difference in δ_{hm} between DCM-BU and DCM-TD to the value of δ_{hm} of DCM-BU. Thus, reduction ratios of 50 and 67% were obtained for DCM-BU in Shanghai and Bangkok soft clays, respectively.

5.5 Distribution of lateral wall movements around the excavation area

The lateral wall movements observed and computed around the sides of the excavation area provided an opportunity to study whether corner effects existed in such a deep and long excavation. Figure 14 shows the relationship between δ_{hm}/H_e and the distance ratio along the west and east long sides and south and north short sides. The distance ratio was measured from the south corner to the north corner and from the west corner to the east corner. The maximum values of δ_{hm}/H_e were 0.8 and 0.6% for the west and east sides of the excavation area, respectively, which were located at the mid-span of each excavation side. The minimum values of δ_{hm}/H_e were 0.05 and 0.1% for the west and east sides of the excavation area, respectively, which were located at the corners of the mid-span of each excavation side. The results observed for the 38-m-deep multistrutted excavation in Shanghai soft clay reported by Lui et al. [26] were also plotted for comparison. There was no significant difference in the values of δ_{hm}/H_e

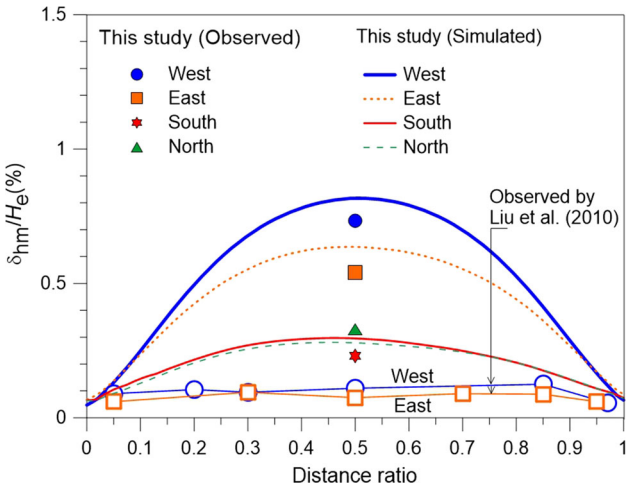

Fig. 14 Relationship between normalized maximum lateral wall movement and distance

for the mid-span and the corner of the excavation area, which were 0.05 to 0.1%H_e, respectively.

A three-dimensional distribution of the lateral wall movements can also be observed in Fig. 14. The support system, stiffness of the strutting system, and length-to-depth and length-to-width ratios should be considered when studying the corner effect of the excavation. The length, width and depth represent the dimensions of the longer side, shorter side and excavation depth of the excavation works, which are 45.3, 28.0 and 7.9 m, respectively, in this study. Studies on corner effects in Singapore and Taiwan clays [8, 22, 25, 31] suggested that a low length-to-depth ratio and smaller length-to-width ratio give rise to more significant corner effects. Lui et al. [26] showed that the length-to-depth ratio and length-to-width ratio were 4.6 and 7.6, respectively, for a deep multistrutted excavation, and no corner effect was found because of the high length-to-width ratio and the sufficient stiffness of the heavy strutting system. However, in this study, the length-to-depth and length-to-width ratios were 5.7 and 1.6, respectively. The low length-to-width ratio compared to that for the excavation system presented by Lui et al. [26] and the insufficient stiffness of the strut system may have contributed to the corner effect in this project.

5.6 Maximum lateral movements versus factor of safety against basal heave (FOS_{base})

Mana and Clough [28] investigated the relationship between δ_{hm} and FOS_{base} using a statistical collection based on several excavations in clay areas around the world (Boston, San Francisco, Chicago, California, Oslo, and others). Some excavations using DW-TD and DW-BU in Shanghai collected by Wang et al. [42], and some databases of excavations using SPWs, DCM-BU and DW-TD

in Bangkok are also cited here. Mana and Clough [28] proposed the limit lines for this relationship. The values of δ_{hm}/H_e for the case in this study are plotted against FOS_{base} in Fig. 15a. The method proposed by Terzaghi [40] was adopted to calculate FOS_{base}. Figure 15a shows that δ_{hm}/H_e tended to decrease with the increasing FOS_{base}. The measured δ_{hm}/H_e in this study falls between the two limit lines, with FOS_{base} values ranging from 1.4 to 1.5. The results indicate that the limits provided by Mana and Clough [28] can also be applicable to DCM-TD in this study. The majority of the data points collected by Wang et al. [42] are within the two limit lines (being nearer to the lower one).

5.7 Influence of system stiffness

Previous studies executed by many researchers, including Rowe [35], Goldberg et al. [9], Clough et al. [7], Potts and Day [34], and Addenbrooke [1], showed that the stiffness of the supporting system is an important factor governing the performance of an excavation. The stiffness of the supporting system relates to many factors, including the bending stiffness of the retaining wall, the axial stiffnesses of the struts, the locations of the struts, and the vertical spacings between the struts. Figure 15b shows the relationship between δ_{hm}/H_e and the system stiffness $EI/\gamma_w h^4$, as defined by Clough et al. [7], for the walls in this study. The design curves, in terms of FOS_{base}, proposed by Clough and O'Rourke [6] are also shown in the figure to illustrate the trends. The stiffness of the wall EI was calculated using a Young's modulus value $E = 20$ MPa for the DCM wall and the second moment of inertia of the wall section, calculated using $I = t^3/12$, where t is the wall thickness, h is the average vertical strut spacing and γ_w is the unit weight of water. Figure 15b shows the value of the system stiffness for DW-TD and DW-BU from the work of Wang et al. [42] for comparison. The system stiffness values for this project were bounded by two curves, $FOS_{base} = 1.2$ and $FOS_{base} = 1.5$, with $FOS_{base} = 1.35$ being an approximate average curve. The DW-TD data points obtained by Wang et al. [42] were between an FOS_{base} of 1.4 and an FOS_{base} of 3.0, with an average FOS_{base} of 2.2. The data points for DW-TD were broadly bounded by the curves $FOS_{base} = 1.1$ and $FOS_{base} = 3.0$. The curve $FOS_{base} = 2.0$ represents an approximate average of this data set. Figure 15b shows that there is a relatively wide scatter of the values of δ_{hm}/H_e for a given system stiffness. However, there is slight evidence of a decreasing trend of δ_{hm}/H_e with increasing system stiffness. This trend is consistent with the findings of Long [27] for case histories in soft soils of significant thicknesses. Moreover, DCM-TD (this study), DW-BU and DW-TD provided the smallest, medium and largest average FOS_{base} values, respectively, which correspond to the average values of δ_{hm}/H_e for various support systems, as shown in Fig. 13.

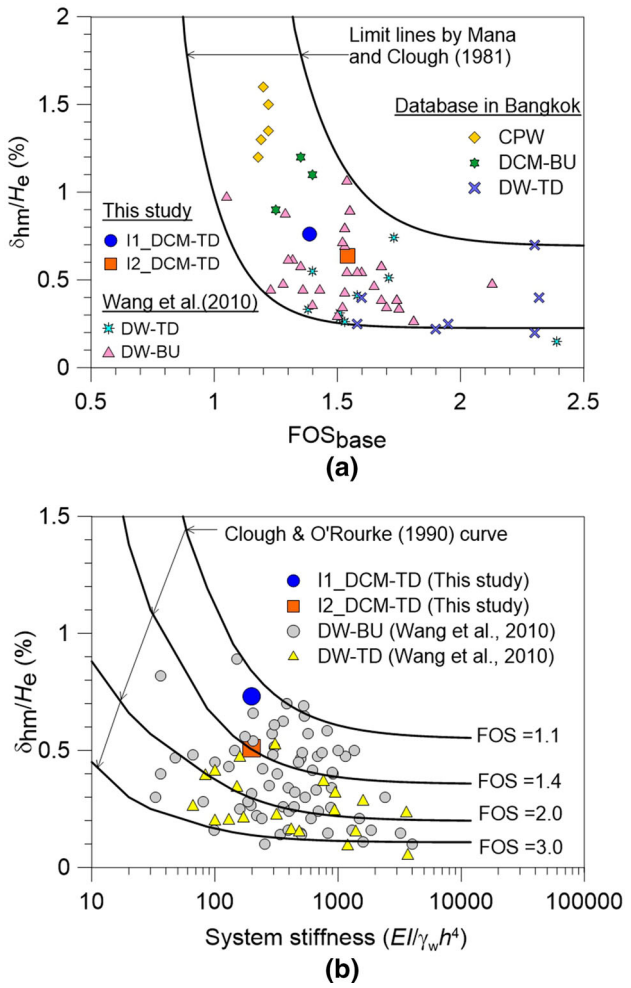

Fig. 15 Normalized maximum lateral wall movement versus: **a** factor of safety against basal heave; **b** system stiffness

5.8 Computed normal forces in the slabs

The distributions of the normal forces per unit length perpendicular to the length of the wall induced in slabs B1-A and B1-B due to the − 7.9-m excavation are presented in Fig. 16. The maximum normal forces in slabs B1-A and B1-B, 130 and 120 kN/m, were located near the centers of the slabs lengthwise. The resultant normal forces in slabs B1-A and B1-B, in units of kN, are summations of the areas under the curves of normal force per unit length versus distance, as shown in Fig. 16. The resultant normal forces in slabs B1-A and B1-B were 4380 and 4370 kN, respectively. Thus, the average resultant normal force was 4375 kN. The summation of the forces in struts S1 to S7 was 2710 kN. Therefore, the difference force was 1665 kN. This force may have been borne by the corners of the walls

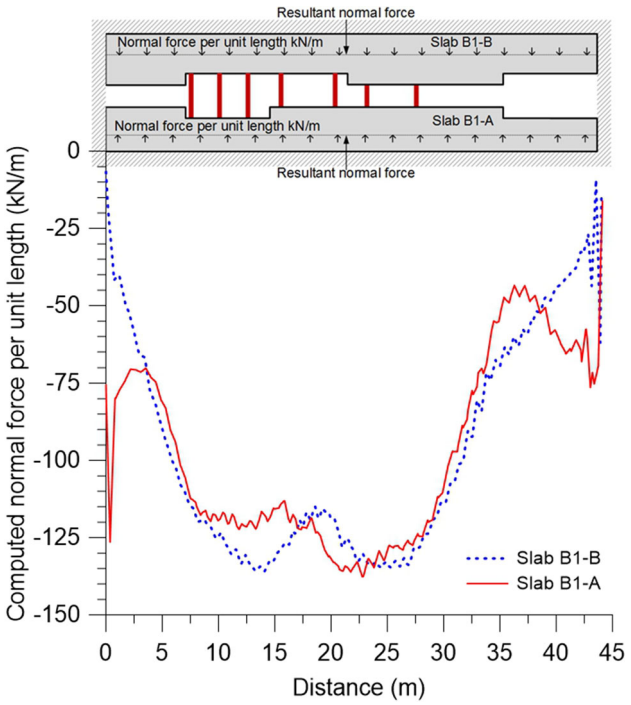

Fig. 16 Distribution of computed normal forces in concrete slabs

in the excavation and the side friction between the slabs and DCM walls. This means that the struts may have borne 62%, with the remaining 38% being borne by the corners and side friction.

5.9 Computed bending moments in the DCM wall

The maximum bending moment (M_{max}) induced in a DCM wall must be known to prevent local failure due to exceeding the moment capacity (M_{yield}) of the DCM wall section. DCM columns typically have higher compressive strengths than tensile and flexural strengths (σ_f). σ_f can be assumed to be $0.15q_{u(DCM)}$ [19] for the design in this study, which corresponds to a σ_f value of 300 kPa. Therefore, a DCM wall can fail when M_{max} reaches M_{yield} [5, 19]. The M_{yield} of a DCM wall in units of kN-m/m can be calculated using the following relationship [15, 19]:

$$M_{yield} = \sigma_f \frac{I}{t/2} \tag{15}$$

Thus, according to Eq. 15, M_{yield} for a DCM wall with a thickness of 2.5 m was 310 kN-m/m. The computed bending moment profiles of the DCM wall located in the middle of each wall side around the excavation area are presented in Fig. 17. The bending moments M_{1-1} and M_{2-2} are the bending moments due to bending around the length and the height of the wall, respectively. The shape is similar to that of a single pile under a lateral load. Between

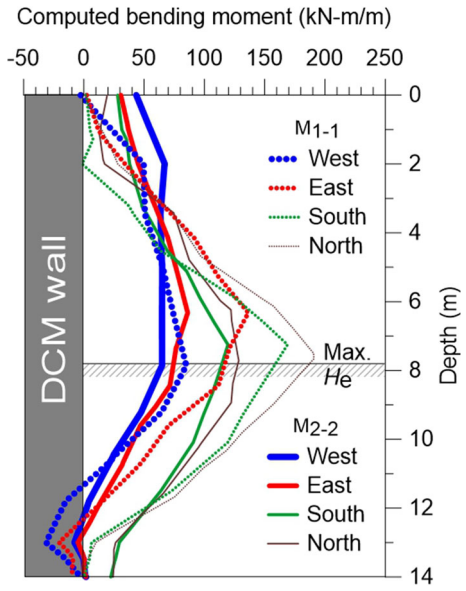

Fig. 17 Computed bending moment profiles for DCM walls

the two long sides of the excavation area, the maximum bending moments M_{1-1} and M_{2-2} were induced on the east side, with magnitudes of 135 and 120 kN-m/m located at depths of 6.1 and 7.1 m, respectively, below the ground surface. In the same way, the wall located at the north side of the excavation provided maximum M_{1-1} and M_{2-2} of 200 and 130 kN-m/m, respectively, at a depth of 7.1 m or 1.0 H_e. Thus, a minimum factor of safety against bending failure ($FS_{bending}$) of 1.55 was obtained for the DCM-TD of this case study. Clearly, the short side provided a maximum M_{1-1} greater than that of the long side by approximately 1.5 times the corresponding length-to-width ratio or 1.6 in this case study.

6 Numerical analysis results of DCM-TD in comparison with those of DCM-BU for the case study

To investigate the effectiveness of the DCM-TD method for deep excavation work, the lateral movement and bending moment profiles of a DCM wall without a permanent concrete slab bracing or a DCM wall using the BU construction method (DCM-BU) were numerically investigated. The DCM-BU method was simulated by omitting the concrete slabs and the temporary struts from the excavation area. The lateral movement profile obtained via 3D finite element analysis, as shown in Fig. 9, was the so-called case study for the analysis presented in the following sections.

Figure 18a shows a comparison of the computed lateral wall movements for the cases with and without concrete

slabs for the walls associated with I1, I2, I3 and I4. The DCM-BU method resulted in considerably larger lateral movements. The shapes of the computed lateral movement profiles for the walls associated with I3 and I4 in Fig. 18a tended to move further toward the excavation, unlike those in the case study. This result confirms that the existence of a slab affected the type of lateral wall movement profiles for the walls associated with I3 and I4, as noted in Sect. 5.1. For the DCM-BU case, the values of δ_{hm} at the top of the wall were approximately 101, 88, 59 and 60 mm for the walls associated with I1, I2, I3 and I4, respectively. Note that the δ_{hm} value for walls associated with I1 and I2 for DCM-BU is larger than the maximum allowable lateral movement of 65 mm for this project. The computed δ_{hm}/H_e ratios for the DCM-BU method were close to the ranges of the observed values for DCM walls in Bangkok and Shanghai shown in Fig. 13. However, when the concrete slabs were installed using the DCM-TD method, the ratio could be reduced to approximately 38, 48, 39 and 39 mm. Therefore, the reduction ratios were 38, 55, 67 and 65% for the walls associated with I1, I2, I3 and I4, respectively. The high reduction ratios reflect the high impact of the existence of a concrete slab bracing. Thus, the DCM-TD method can reduce lateral movement, with an average reduction ratio of 56% for this project.

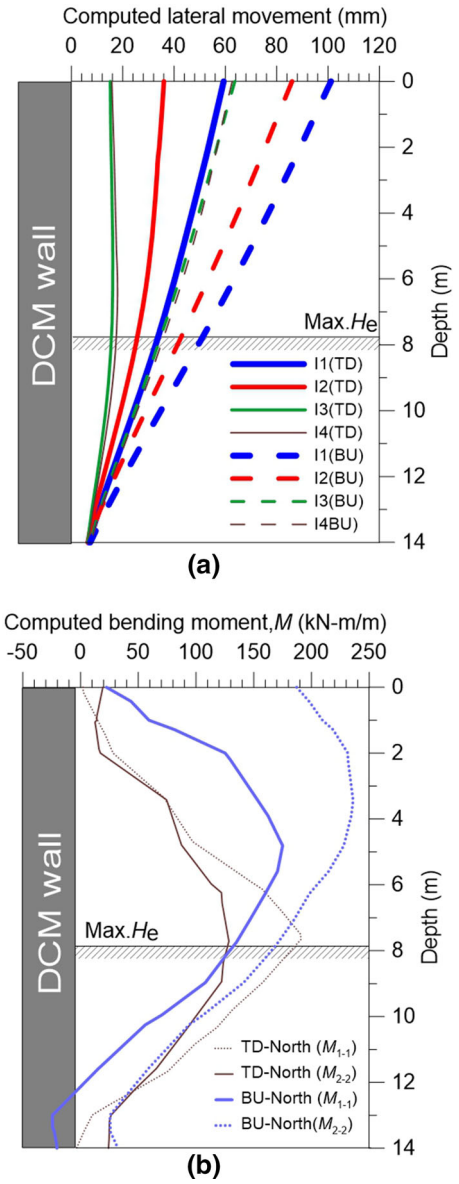

Fig. 18 Comparison of **a** computed lateral wall movement profiles and **b** bending moment profiles for DCM-TD and DCM-BU

The bending moment profiles of the DCM-TD and DCM-BU methods for the northern side of the excavation area are presented in Fig. 18b. The bending moment M_{2-2} of the DCM walls with and without the concrete slab was significantly different in both magnitude and shape, especially at depths above the excavation depth. The location of maximum moment M_{2-2} changed from a depth of 8 m to a depth of 3 m for DCM-TD and DCM-BU, respectively. The magnitude of the maximum moment M_{2-2} changed from 130 to 240 kN-m/m for DCM-TD and DCM-BU, respectively. However, there was an insignificant change in bending moment M_{1-1}. The magnitude of the maximum moment M_{1-1} changed from 200 to 180 kN-m/m for DCM-TD and DCM-BU, respectively. Note that the construction method can change the magnitude of M_{max} from M_{1-1} to M_{2-2}, namely M_{1-1} is minimum for DCM-BU, whereas M_{2-2} is minimum for DCM-TD because of the existence of a concrete slab. A minimum $FS_{bending}$ of 1.29 was obtained for DCM-BU, which is smaller than that for DCM-TD and is lower than the $FS_{bending}$ value of 1.50 required for this project. Thus, DCM-BU with four rows of DCM walls is unsuitable for this project based on the performance-based design.

As mentioned above, both the lateral wall movement and the bending moments (particularly M_{2-2}) in a DCM wall above the excavation level drastically decrease when the concrete slab is introduced. This result reveals that the lateral earth pressure applied to the wall has been substantially transferred to the concrete slabs. It also implies the potential of implementing the DCM-TD method for excavations at greater depths when the wall thickness is kept constant.

7 Numerical investigation on applicability and future potential of DCM-TD compared to DCM-BU for greater excavation depths

This section presents the applicability of the DCM-TD method to investigate its future potential for greater excavation depths. Thus, the excavation depths used in additional analyses increase from 7.9 to 10.9 and 13.9 m, which

correspond to three and four levels of slabs, respectively. The thickness of the slabs and number of struts at each level were assumed to be the same as in the case study, as shown in Fig. 19. In addition, the design of a deep excavation work in an urban area is limited to an insufficient space close to a property line. Thus, the thickness of the DCM wall is an important factor for designing using the DCM-TD and DCM-BU methods. The wall thickness for this project was limited to 2.5 m, or four rows of a DCM wall, because of the insufficient space. M_{max} in the DCM wall is an important design parameter because it establishes the wall thickness required to maintain a performance-based design. Based on Eq. 1, M_{yield} depends on the wall thickness, whereas σ_f is a property of the soil–cement material. Assuming that all DCM walls in this study comprise a homogeneous and isotropic material, the value of M_{yield} for various wall thicknesses can be determined using Eq. 1 and, as shown in Fig. 20, using the same σ_f value of 300 kPa. These values are used for comparison with the M_{max} value computed for the DCM wall based on 3D-FEM.

First, an appropriate wall thickness must be determined based on the minimum $FS_{bending}$ of 1.50 to prevent bending failure of the wall. Then, δ_{hm} must be calculated to verify that the induced δ_{hm} is smaller than 65 mm based on the performance-based design. Figure 21a shows the effects of the DCM wall thickness on the minimum $FS_{bending}$ at various excavation depths for DCM-BU and DCM-TD.

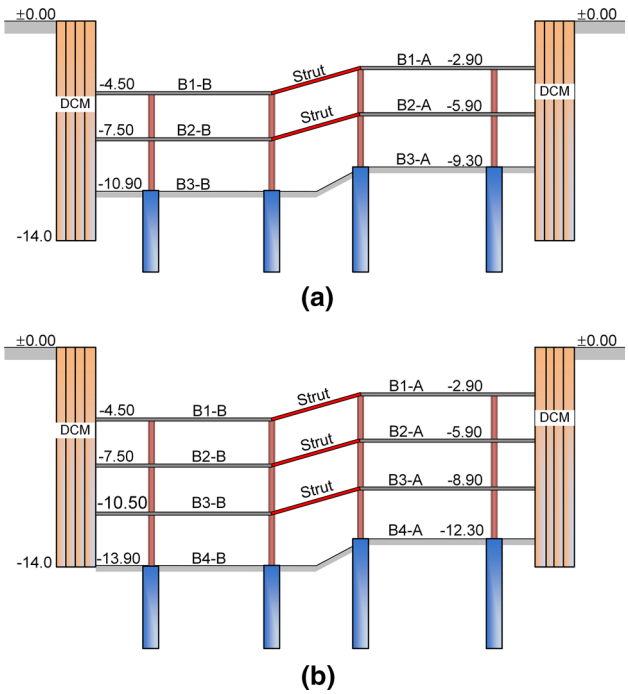

Fig. 19 Cross-sectional view of DCM-TD for **a** H_e = 10.9 m and H_e = 13.9 m

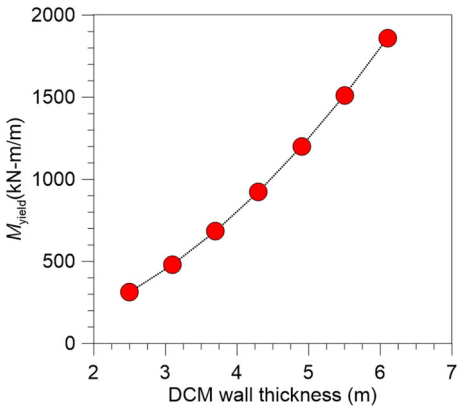

Fig. 20 M_{yield} versus DCM wall thickness

The numerical results show that the $FS_{bending}$ of the DCM wall increases with increasing wall thickness because of the increase in M_{yield} for both DCM-TD and DCM-BU and that the incremental rates for DCM-BU were higher than those for DCM-TD. This result implies that DCM-TD has an advantage in distributing induced bending moments and lateral loads from a deep excavation. Figure 21b presents only the corresponding δ_{hm} for a DCM wall providing a minimum $FS_{bending}$ value greater than 1.50, and the value of δ_{hm} decreases with the increasing wall thickness because of the increase in wall rigidity [42] for both DCM-TD and DCM-BU. Because of the existence of concrete slabs, the values of δ_{hm} for the same wall thickness at different H_e are insignificantly different. The values of δ_{hm} for the wall are almost unchanged with increasing excavation depths, unlike the DCM-BU method, because of the very high stiff lateral support of the concrete slab. This system is more suitable for deep excavations in urban environments, particularly under conditions of limited perimeter space and adjacent existing structures. In addition, the DCM-TD method for the field case study (H_e = 7.9 m) requires almost half the wall thickness of the DCM-BU method to obtain the required δ_{hm} value of 65 mm. In the same manner, a wall thickness of 3.1 m is sufficient for DCM-TD for H_e values greater than 7.9 m, while wall thicknesses of 4.9 and 6.1 m are required for DCM-BD for H_e values of 10.9 and 13.9 m, respectively.

To evaluate the effectiveness of DCM-TD considering the effect of the wall thickness and H_e, the reduction ratio versus the wall thickness for various H_e values is presented in Fig. 21c. The reduction ratio values decrease with increasing wall thickness for all H_e, which implies that DCM-TD is appropriate for thin DCM walls. The reduction ratios increase with increasing H_e for the same wall thickness, and the average values of the reduction ratios are 33, 44 and 57% for H_e of 7.9, 10.9 and 13.9 m, respectively, which reflects the fact that DCM-TD is more effective for deeper excavations.

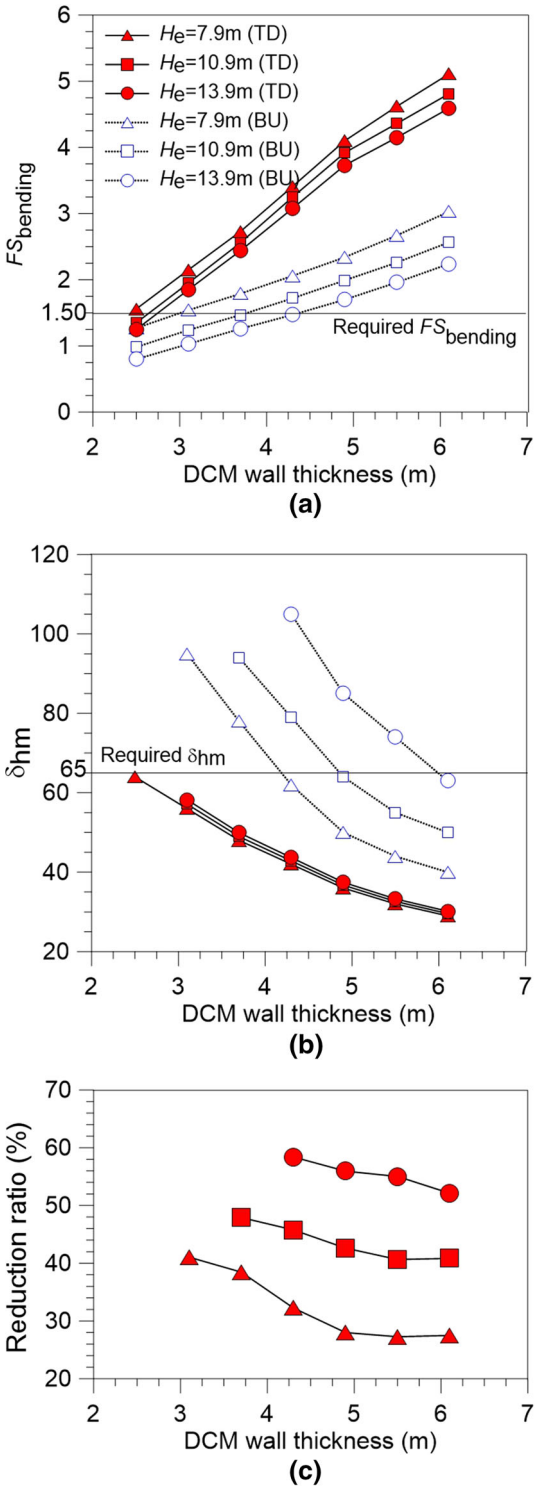

Fig. 21 Effect of DCM wall thickness and excavation depth on **a** $FS_{bending}$, **b** δ_{hm} and **c** reduction ratio

Figure 22 shows the effect of wall thickness on the average normal forces in the struts and the slabs for various H_e for DCM-TD, which are defined as the total normal forces in the struts divided by the total numbers of struts

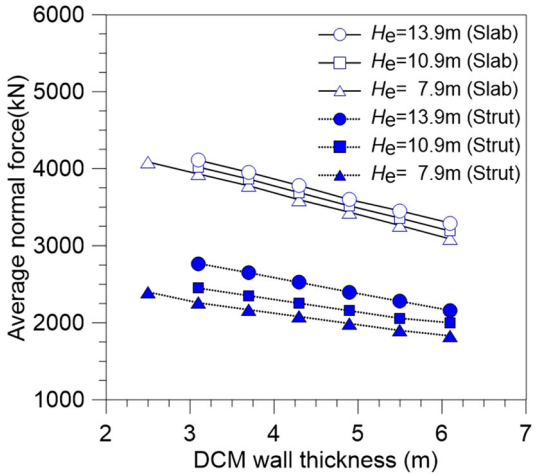

Fig. 22 Effect of DCM wall thickness and excavation depth on average normal force in strut and slab

and the total normal forces in the slabs divided by the total numbers of slabs, respectively. The figure shows that the wall thickness has a substantial effect on the forces in struts and slabs. As expected, the results show that the overall tendency is the reduction in forces in struts and slabs with increasing wall rigidity for various H_e. In addition, the forces in the struts and slabs increase with the increasing H_e for the same wall thickness, which confirms that a concrete slab requires a greater lateral load to maintain similar values of δ_{hm} for different H_e, as shown in Fig. 21b. The differences between the forces in the slabs and struts or the remaining forces borne by the corners and side friction were approximately 38, 33 and 29% for H_e of 7.9, 10.9 and 13.9 m, respectively.

8 Summary and conclusions

A case study of a DCM wall applied using a top-down construction method (DCM-TD) for a deep excavation in soft Bangkok clay has been reported. The lateral movements of the wall system and the strut forces at the proposed excavation depth were observed. A calibration of laboratory test results using a hardening soil model was performed to obtain the best parameters for simulating the behavior of the foundation soils and DCM column. The magnitude of the maximum lateral movement of the wall (δ_{hm}) was compared with the results for various types of supports used in previous studies. An analysis of the results of the case study was then conducted to assist in understanding the wall behavior in terms of the lateral movements and the forces in structural members using the three-dimensional finite element analysis. Finally, a numerical investigation of the applicability and future potential of DCM-TD at greater depths in comparison with the DCM

wall using the bottom-up construction method (DCM-BU) was carried out. The following conclusions were drawn based on the observed and simulated results:

1. The DCM-TD in this study provided a measured maximum δ_{hm} of 58 mm and a minimum $FS_{bending}$ of 1.55 by assuming that $\sigma_f = 0.15q_{u(DCM)}$, which meets the criteria for performance-based designs for deep excavation works in the urban Bangkok area, namely δ_{hm} and $FS_{bending}$ values equal to 65 mm and 1.50, respectively. Based on a design with the mentioned criteria, no damage to the ground near the excavation area was observed for the DCM-TD used for this study.
2. The upper bound of the observed δ_{hm}, $0.73\%H_e$, for a DCM-TD was within the average values of the observed δ_{hm} for DW-BU and DCM-BU obtained in previous studies. The mean value of δ_{hm} for this study, $0.45\%H_e$, reflects that the observed effectiveness of DCM-TD was superior to that of DCM-BU by as much as three times but close to that of DW-BU, with a difference of as much as 0.8 times.
3. The δ_{hm}/H_e value measured in this study falls between the two limit lines presented by Mana and Clough [28], with an average FOS_{base} value of 1.45, whereas the average FOS_{base} value obtained from the relationship between δ_{hm}/H_e and the system stiffness is 1.35, implying that this wall system provides a high potential resistance against basal heave. The DCM with the TD method (this study), DW-BU and DW-TD provided the smallest, medium and largest average FOS_{base} values, respectively.
4. Based on the strut forces observed in this study, a minimum factor of safety against structural failure of 6.7 was obtained, which was confirmed by a performance-based design. The excess bending moments were induced in the strut due to the effect of installation with an inclination, which produced maximum excess bending moments of 62 kN-m. However, the excess bending moments were compensated by a high value of the factor of safety against structural failure.
5. Sixty-two percent of the total normal forces perpendicular to the length of the slabs were shared by the struts, and the remaining 38% of the forces were shared by the corners and side friction.
6. The computed maximum bending moment induced in the DCM-TD wall is the bending moment due to bending around the length of the wall. The short side provided a maximum M_{1-1} greater than the long side by approximately 1.5 times corresponding to the length-to-width ratio or 1.6 in this case study.
7. The numerical results of the case study show that the concrete slab used in the TD construction had a large effect on the lateral wall movements and bending moment in the DCM walls. With the concrete slab, the lateral movements were reduced, with an approximate average reduction ratio of 62% based on four locations of δ_{hm} around the excavation area. The existence of the slab also changed the magnitude of M_{max} from M_{1-1} to M_{2-2} and reduced the magnitude of M_{2-2} by as much as 1.85 times.
8. For the specific case study of the DCM-TD wall in soft Bangkok clay, a series of parametric studies of excavation at depths greater than that of the case study indicate that DCM-TD provides insignificant changes in δ_{hm}, as the system stiffness is large enough such that any further increase in H_e in the range of this study will not increase the value of δ_{hm} further. The induced lateral forces and bending moments are thus mainly absorbed by the slabs and struts, which is confirmed by higher loads in the concrete slabs and struts for larger values of H_e.
9. The DCM-TD method for the field case study (H_e = 7.9 m) requires almost half the wall thickness of the DCM-BU method to obtain the required δ_{hm} value of 65 mm. In the same manner, a wall thickness of 3.1 m is sufficient for DCM-TD for H_e values greater than 7.9 m, while wall thicknesses of 4.9 and 6.1 m are required for DCM-BD for H_e values of 10.9 and 13.9 m, respectively.
10. An evaluation of the effectiveness of DCM-TD compared to that of DCM-BU without the creep time effect showed that the reduction ratios for lateral wall movement are 33, 44 and 56% for H_e of 7.9, 10.9 and 13.9 m, respectively, based on the computed maximum δ_{hm}. This reveals the future potential of implementing DCM-TD for deep excavation works in urban environments.

Acknowledgements This research was funded by King Mongkut's University of Technology North Bangkok under Contract No. KMUTNB-GOV-59-03. The authors also extend their appreciation to the Thailand Research Fund (TRF) under Basic Research Grant No. BRG6080011.

Appendix: Creep effect on lateral wall movements

Figure 23 shows the creep effect on the lateral movements of the walls associated with I1 and I2 for excavation stages 7 and 9 and stages 4 and 6, respectively. As shown, the creep effect is insignificant for this project.

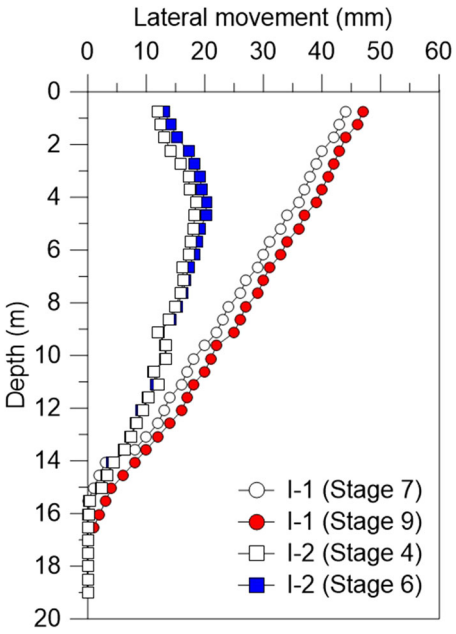

Fig. 23 Creep effect on the lateral movements of the walls

References

1. Addenbrooke TI (1994) A flexibility number for the displacement controlled design of multi propped retaining walls. Gr Eng 27:41–45
2. Arboleda-Monsalve LG, Finno RJ (2015) Influence of concrete time-dependent effects on the performance of top-down construction. J Geotech Geoenviron Eng 141:985–994. https://doi.org/10.1061/(ASCE)GT.1943-5606.0001260
3. Bergado DT, Teerawattanasuk C, Youwai S, Voottipruex P (2000) Finite element modeling of hexagonal wire reinforced embankment on soft clay. Can Geotech J 37:1209–1226. https://doi.org/10.1139/t00-065
4. Borja RI (2013) Plasticity modeling and computation. Springer, Berlin-Heidelberg
5. Chai J, Shrestha S, Hino T, Ding W, Kamo Y, Carter J (2015) 2D and 3D analyses of an embankment on clay improved by soil–cement columns. Comput Geotech 68:28–37. https://doi.org/10.1016/j.compgeo.2015.03.014
6. Clough GW, O'Rourke TD (1990) Construction induced movements of in situ walls. In: Proceedings of the ASCE conference on design and performance of earth retaining structures. American Society of Civil Engineers, New York, pp 439–470
7. Clough GW, Smith EM, Sweeney BP (1989) Movement control of excavation support systems by iterative design. In: Proceedings of the ASCE foundation engineering: current principles and practice, vol 2. American Society of Civil Engineers, New York, pp 869–884
8. Finno RJ, Blackburn JT, Roboski JF (2007) Three-dimensional effects for supported excavations in clay. J Geotech Geoenviron Eng 133:30–36. https://doi.org/10.1061/(ASCE)1090-0241(2007)133:1(30)
9. Goldberg DT, Jaworski WE, Gordon MD (1976) Lateral support systems and underpinning. Rep No. FHWA-RD-75-129. Federal Highway Administration, Washington
10. Hou YM, Wang JH, Zhang LL (2009) Finite-element modeling of a complex deep excavation in Shanghai. Acta Geotech 4:7–16. https://doi.org/10.1007/s11440-008-0062-3
11. Hsieh P, Ou C, Lin Y (2013) Three-dimensional numerical analysis of deep excavations with cross walls. Acta Geotech 8:33–48. https://doi.org/10.1007/s11440-012-0181-8
12. Hsiung BB, Yang K, Aila W, Hung C (2016) Three-dimensional effects of a deep excavation on wall deflections in loose to medium dense sands. Comput Geotech 80:138–151. https://doi.org/10.1016/j.compgeo.2016.07.001
13. Huang J, Han J (2009) 3D coupled mechanical and hydraulic modeling of a geosynthetic-reinforced deep mixed column-supported embankment. Geotext Geomembr 27:272–280. https://doi.org/10.1016/j.geotexmem.2009.01.001
14. Ignat R, Baker S, Larsson S, Liedberg S (2015) Two- and three-dimensional analyses of excavation support with rows of dry deep mixing columns. Comput Geotech 66:16–30. https://doi.org/10.1016/j.compgeo.2015.01.011
15. Jamsawang P, Bergado DT, Voottipruex P (2011) Field behaviour of stiffened deep cement mixing piles. Proc Inst Civ Eng Ground Improv 164:33–49. https://doi.org/10.1680/grim.900027
16. Jamsawang P, Voottipruex P, Boathong P, Mairaing W, Horpibulsuk S (2015) Three-dimensional numerical investigation on lateral movement and factor of safety of slopes stabilized with deep cement mixing column rows. Eng Geol 188:159–167. https://doi.org/10.1016/j.enggeo.2015.01.017
17. Jamsawang P, Voottipruex P, Jongpradist P, Bergado DT (2015) Parameters affecting the lateral movements of compound deep cement mixing walls by numerical simulations and parametric analyses. Acta Geotech 10:797–812. https://doi.org/10.1007/s11440-015-0417-5
18. Jamsawang P, Boathong P, Mairaing W, Jongpradist P (2016) Undrained creep failure of a drainage canal slope stabilized with deep cement mixing columns. Landslides 13:939–955. https://doi.org/10.1007/s10346-015-0651-9
19. Jamsawang P, Yoobanpot N, Thanasisathit N, Voottipruex P, Jongpradist P (2016) Three-dimensional numerical analysis of a DCM column-supported highway embankment. Comput Geotech 72:42–56. https://doi.org/10.1016/j.compgeo.2015.11.006
20. Jongpradist P, Jumlongrach N, Youwai S, Chucheepsakul S (2010) Influence of fly ash on unconfined compressive strength of cement-admixed clay at high water content. J Mater Civ Eng 22:49–58. https://doi.org/10.1061/(ASCE)0899-1561(2010)22:1(49)
21. Jongpradist P, Kaewsri T, Sawatparnich A, Suwansawat S, Youwai S, Kongkitkul W, Sunitsakul J (2013) Development of tunneling influence zones for adjacent pile foundations by numerical analyses. Tunn Undergr Space Technol 34:96–109. https://doi.org/10.1016/j.tust.2012.11.005
22. Lee F, Yong K, Quan KCN, Chee K (1998) Effect of corners in strutted excavations: field monitoring and case histories. J Geotech Geoenviron Eng 124:339–349. https://doi.org/10.1061/(ASCE)1090-0241(1998)124:4(339)
23. Likitlersuang S, Surarak C, Wanatowski D, Oh E, Balasubramaniam A (2013) Finite element analysis of a deep excavation: a case study from the Bangkok MRT. Soils Found 53:756–773. https://doi.org/10.1016/j.sandf.2013.08.013
24. Lim A, Hsieh P, Ou C (2016) Evaluation of buttress wall shapes to limit movements induced by deep excavation. Comput Geotech 78:155–170. https://doi.org/10.1016/j.compgeo.2016.05.012
25. Liu KX (1995) Three dimensional analysis of deep excavation in soft clay. Masters, National University of Singapore
26. Liu GB, Jiang RJ, Ng CWW, Hong Y (2011) Deformation characteristics of a 38 m deep excavation in soft clay. Can Geotech J 48:1817–1828. https://doi.org/10.1139/t11-075
27. Long M (2001) Database for retaining wall and ground movements due to deep excavations. J Geotech Geoenvironmental Eng 127:203–224. https://doi.org/10.1061/(ASCE)1090-0241(2001)127:3(203)

28. Mana AI, Clough GW (1981) Prediction of movements for braced cuts in clay. J Geotech Eng (Div) 6:759–777
29. Moormann C (2004) Analysis of wall and ground movements due to deep excavations in soft soil based on a new worldwide database. Soils Found 44:87–98. https://doi.org/10.3208/sandf.44.87
30. Ou C, Hsieh P, Chiou D (1993) Characteristics of ground surface settlement during excavation. Can Geotech J 30:758–767. https://doi.org/10.1139/t93-068
31. Ou C, Liao J, Lin H (1998) Performance of diaphragm wall constructed using top-down method. J Geotech Geoenviron Eng 124:798–808. https://doi.org/10.1061/(ASCE)1090-0241(1998)124:9(798)
32. Ou CY, Hsieh PG, Lin YL (2013) A parametric study of wall deflections in deep excavations with the installation of cross walls. Comput Geotech 50:55–65. https://doi.org/10.1016/j.compgeo.2012.12.009
33. Phutthananon C, Jongpradist P, Yensri P, Jamsawang P (2018) Dependence of ultimate bearing capacity and failure behavior of T-shaped deep cement mixing piles on enlarged cap shape and pile strength. Comput Geotech 97:27–41. https://doi.org/10.1016/j.compgeo.2017.12.013
34. Potts DM, Day RA (1991) The effect of wall stiffness on bending moments. In: The 4th international conference on piling and deep foundations, pp 435–444
35. Rowe PW (1952) Anchored sheet-pile walls. Proc Inst Civ Eng 1:27–70. https://doi.org/10.1680/iicep.1952.10942
36. Schanz T, Vermeer PA, Bonnier PG (1999) The hardening-soil model: formulation and verification. In: Brinkgreve RBJ (ed) Beyond 2000 in computational geotechnics. Balkema, Rotterdam, pp 281–290
37. Sexton BG, McCabe BA (2013) Numerical modelling of the improvements to primary and creep settlements offered by granular columns. Acta Geotech 8:447–464. https://doi.org/10.1007/s11440-012-0205-4
38. Shao Y, Macari EJ, Cai W (2005) Compound deep soil mixing columns for retaining structures in excavations. J Geotech Geoenviron Eng 131:1370–1377. https://doi.org/10.1061/(ASCE)1090-0241(2005)131:11(1370)
39. Surarak C, Likitlersuang S, Wanatowski D, Balasubramaniam A, Oh E, Guan H (2012) Stiffness and strength parameters for hardening soil model of soft and stiff Bangkok clays. Soils Found 52:682–697. https://doi.org/10.1016/j.sandf.2012.07.009
40. Terzaghi K (1943) Theoretical soil mechanics. Wiley, New York
41. Wang ZW, Ng CW, Liu GB (2005) Characteristics of wall deflections and ground surface settlements in Shanghai. Can Geotech J 42:1243–1254. https://doi.org/10.1139/t05-056
42. Wang JH, Xu ZH, Wang WD (2010) Wall and ground movements due to deep excavations in Shanghai soft soils. J Geotech Geoenviron Eng 136:985–994. https://doi.org/10.1061/(ASCE)GT.1943-5606.0000299
43. Wonglert A, Jongpradist P (2015) Impact of reinforced core on performance and failure behavior of stiffened deep cement mixing piles. Comput Geotech 69:93–104. https://doi.org/10.1016/j.compgeo.2015.05.003
44. Wonglert A, Jongpradist P, Jamsawang P, Larsson S (2018) Bearing capacity and failure behaviors of floating stiffened deep cement mixing columns under axial load. Soils Found. https://doi.org/10.1016/j.sandf.2018.02.012
45. Zhang W, Goh ATC, Xuan F (2015) A simple prediction model for wall deflection caused by braced excavation in clays. Comput Geotech 63:67–72. https://doi.org/10.1016/j.compgeo.2014.09.001
46. Zhao C, Lavasan AA, Barciaga T, Zarev V, Datcheva M, Schanz T (2015) Model validation and calibration via back analysis for mechanized tunnel simulations—the western Scheldt tunnel case. Comput Geotech 69:601–614. https://doi.org/10.1016/j.compgeo.2015.07.003